Hindawi
Structural Control and Health Monitoring
Volume 2023, Article ID 9526244, 21 pages
https://doi.org/10.1155/2023/9526244

Research Article

Performance Examination of Nonlinear Signal-Based Control in Shake Table Experiments with Sliding Structures

Ryuta Enokida,[1] **Kohju Ikago**,[1] **Jia Guo**,[2] **and Koichi Kajiwara**[3]

[1]*International Research Institute of Disaster Science, Tohoku University, Sendai 980-0845, Japan*
[2]*Department of Agricultural and Environmental Engineering, Kyoto University, Kyoto 606-8502, Japan*
[3]*E-Defense, National Research Institute for Earth Science and Disaster Resilience, Nishikameya 1501-21, Mitsuda, Shijimi-cho Miki 673-0515, Hyogo, Japan*

Correspondence should be addressed to Ryuta Enokida; enokida@irides.tohoku.ac.jp

Received 22 December 2022; Revised 19 March 2023; Accepted 10 June 2023; Published 28 June 2023

Academic Editor: Łukasz Jankowski

This study examines nonlinear signal-based control (NSBC) in shake table experiments with sliding structures, which have an isolation effect during an earthquake. NSBC uses a nonlinear signal obtained from the outputs of a controlled system and its linear model under the same input. Owing to the presence of the linear model, NSBC controllers are described by transfer functions, even for controlling nonlinear systems. NSBC achieved excellent control of the shake table in experiments with a specimen having nonlinear characteristics such as yielding of structural components. A sliding structure placed on a shake table significantly jeopardises its control because the nonlinear severity of sliding is greater than yielding, and its compensation has not yet been fully developed. Therefore, this study introduces NSBC into shake table experiments with sliding structures along with its linear model design to enhance their robustness, utilising the analysis stability to evaluate the design. Numerical simulations with a shake table with a sliding structure with a friction coefficient of 0.22 demonstrate the excellent performance of NSBC in table acceleration control. However, inversion-based control (IBC), a basic compensation approach, shows its ineffectiveness. In actual shake table experiments with a sliding structure with a friction coefficient of 0.2, NSBC with a reasonable linear model achieved excellent table acceleration control with almost 100% accuracy, whereas IBC was ineffective. This study clarifies that NSBC can solve the problem of control degradation caused by a sliding structure placed on the table.

1. Introduction

In the field of earthquake engineering, a shake table plays an important role in examining the seismic performance of building structures and infrastructure [1, 2]. In a shake table experiment, a specimen placed on the table is excited by reproducing a predetermined signal, which is typically derived from seismic acceleration data recorded during an earthquake in the past or from artificially generated data for experimental purposes. The reproduction of the excitation is a matter of control, and its accuracy must be sufficiently high to precisely examine the specimen under the anticipated situations or conditions.

Shake tables are commonly controlled using a proportional-integral-derivative (PID) method applied to table displacement or similar methods such as three-variable control (TVC) [3, 4]. These controllers are designed such that the table dynamics, including the controller, obtain the expected dynamic characteristics, such as second- or higher-order dynamics. When a heavy specimen is placed on the table, the table dynamics affected by the interaction significantly differ from those without the specimen [5, 6]. To compensate for this influence, an inversion of the dynamics, which is referred to as inversion-based control (IBC) in this study, is commonly employed as a feedforward controller acting on reference signals [3, 4, 7]. This approach is effective only for cases in

which the specimen is a linear system whose characteristics are accurately reflected in the feedfoward controller.

In shake table experiments, nonlinear characteristics within an actuation system and the structure to be examined degrade its control. Shake tables driven by hydraulic actuators exhibit nonlinearity derived from the hydraulic fluid, servo-valves, and friction of cylinders within the actuation system [8–13]. Shake table experiments are mainly conducted to observe seismic damage or failures in structures or nonlinear characteristics in earthquake protection devices [2]. The appearance of nonlinear characteristics during shaking is essential. When this occurs in a heavy specimen placed on a table, the nonlinear characteristics degrade the control, leading to instability in the worst case. An iterative approach based on IBC [3, 14] is occasionally employed to compensate for such nonlinear characteristics, but it is mainly limited to fixed characteristics without uncertainty. An effective approach based on feedback actions is required to accurately control shake tables, regardless of the type of nonlinear characteristics. It will be beneficial to its advanced technique, substructuring shake table experimentation, which is a prime subject actively studied in earthquake engineering [15–21].

To the control issue of shake table experiments, minimal control synthesis (MCS) [22, 23], which is a type of model reference adaptive control [24], was intensively studied and applied in various shake tables, mainly focussing on nonlinear characteristics within the actuation system [25–27]. The success of MCS has led to the class of adaptive control methods being a major tool for shake table experiments involving nonlinear characteristics [28–32]. However, adaptive control approaches still have challenging issues, particularly for systems with large unmodelled dynamics or rapid parameter variations. These issues have been addressed via enhancements with additional techniques (e.g., real-time parameter estimation [33] or a backstepping technique [34–37]).

A class of improvements in IBC is another research topic in shake table experiments with nonlinearity. Model-based control (MBC), which employs an error feedback action into IBC, has been actively investigated for shake table control [13, 38–40]. MBC with a linear quadratic Gaussian controller as its error feedback action has been applied to a shake table sustaining a specimen equipped with wooden braces that display nonlinear characteristics over its elastic range [39, 41].

Nonlinear signal-based control (NSBC) [42–45], which has been specifically established for nonlinear system control, is defined as the addition of a nonlinear signal feedback action into IBC. NSBC uses a nonlinear signal obtained from the outputs of a controlled system and its linear model under the same input. As NSBC relies on a linear model rather than a controlled system, its controllers are described by transfer functions, even for nonlinear system control. NSBC is advantageous because it requires only the output of a controlled part in the controlled system for its feedback action and does not require the outputs of other parts (e.g., structural responses in shake table experiments) for the action. The effectiveness of NSBC has been demonstrated by dynamic substructuring experiments [46, 47] and shake table experiments [44, 48, 49]. The first application of NSBC to shake table experiments [44] was performed using a single-axis shake table with a steel structure, whose weight was equal to the table weight. In the experiments, NSBC successfully realised an expected earthquake excitation with almost 100% accuracy, even when the structure on the table displayed severe nonlinear characteristics owing to the yielding of its structural components.

Regarding the severity of nonlinearity, sliding is one of the most severe phenomena observed in earthquake engineering. In addition, the occurrence of sliding has a positive impact on the seismic damage mitigation of structures [50–52], and modern sliding isolation systems [53–55] that intentionally utilise this aspect have become prominent earthquake protection devices in this field [56]. The excellence of sophisticated systems has led to the development of similar sliding systems based on primitive materials that are expected to exhibit an isolation effect during large earthquakes. These developments have been actively investigated along with studies on the friction of various materials, such as scraped tyres [57–59], sand [60], and common construction materials [61–64], which are typically tested in shake table experiments.

The sliding of a specimen on a shake table affects the table control, and its influence increases as the weight of the specimen increases [65]. When a heavy structure with a certain friction coefficient slides on a shake table, the sliding structure is shaken by an excitation that is completely different from the required one. A countermeasure to this control problem has not yet been fully developed, mainly because of the severities of the nonlinear characteristics caused by the friction and the interaction between the table and the sliding structure.

As NSBC can be a solution to this problem, this study numerically and experimentally examines the performance of NSBC in shake table experiments with a sliding structure with a friction coefficient of approximately 0.2. This study is an advancement of the preceding studies [44, 65], and its novelty is summarised as follows.

(i) This study introduces a new linear model design where parameters in a linear model of a controlled system including a sliding structure are intentionally tuned to enhance the robustness of NSBC. In addition, this study introduces a method to approximately analyse the stability of NSBC for a shake table with a sliding structure. The NSBC stability analysis based on the Nyquist stability criterion can be used to evaluate stability margins obtained from different linear models.

(ii) This study numerically and experimentally demonstrates the effectiveness of NSBC in shake table experiments with a sliding structure, which displays frictional behaviour whose nonlinear severity is greater than yielding of structural components and the friction behaviour of a sliding mass. This study clarifies that NSBC can solve the problem of control degradation caused by the sliding of the structure on the table.

The remainder of this paper is organised as follows. Section 2 studies the influence of a sliding structure on shake table control and describes the application of NSBC in shake table experiments with a sliding structure with N-storeys.

Section 3 numerically examines the control performance of NSBC in shake table experiments with a single-degree-of-freedom (SDOF) structure placed on a sliding mass, along with its comparison with IBC. Section 4 introduces the control performance of NSBC and IBC in actual shake table experiments with a sliding structure consisting of a single-storey steel structure and a sliding mass placed on a graphite-lubricated sliding interface. Finally, Section 5 presents the conclusions of this study.

2. Shake Table Control Degradation Caused by Nonlinearity and Its Compensation by NSBC

2.1. Influence of Sliding Structures on Shake Table Control. The sliding of the two systems, as shown in Figures 1(a) and 1(b), is first formulated, followed by the formulation of the sliding system on a shake table, as shown in Figure 1(c), to investigate their interaction and influence on shake table control.

2.1.1. Sliding Structures. A mass placed on the ground, as shown in Figure 1(a), slides when an applied force in its sliding interface exceeds the maximum static friction of the sliding mass. When the force is caused by ground movement, which occurs during an earthquake, the slip and stick states of the mass are described by the following equation:

$$m_1\ddot{y}_1(t) = \begin{cases} F_{ex}(t)\left(=m_1\ddot{y}_g(t)\right)\left(\text{stick state: } \dot{x}_1(t)=0\right), \\ -F_{\mu v}(t)\operatorname{sgn}\left(\dot{x}_1(t)\right)\left(\text{slip state: } \dot{x}_1(t)\neq 0\right), \end{cases} \tag{1}$$

where t is the time variable; m_1 is the sliding mass; $\{y_1, y_g\}$ is the set of mass displacement and ground displacement in the absolute coordinate, respectively; $x_1 (= y_1 - y_g)$ is the sliding displacement of the mass; $\operatorname{sgn}(a) = \{1\ (a>0), 0\ (a=0), -1\ (a<0)\}$; and $F_{\mu v}$ is the kinematic friction. When the kinematic friction $F_{\mu v}$ is equal to the maximum static friction $F_{\mu s}$, it becomes $F_{\mu v} = F_{\mu s} = \mu_{\max} m_1 g$, where $\mu_{\max}$ is the maximum static friction, and g is the gravitational acceleration.

Equation (1) rigorously distinguishes the states of stick and slip by $\dot{x}_1(t) = 0$ and $\dot{x}_1(t) \neq 0$. This distinction is not practical for numerical simulations because of the strict requirement of zero velocity, which cannot be realised in computation. Therefore, this study employs the Karnopp model [66–68], which distinguishes between the two states by the limit velocity on the stick state, ε_v. Subsequently, the friction for the stick and slip states in equation (1) can be uniformly expressed as follows:

$$F_1(t)\left(=m_1\ddot{y}_1(t)\right) = F_{ex}(t)\left(1-H(t)\right) - F_{\mu v}(t)\operatorname{sgn}\left(\dot{x}_1(t)\right)H(t), \tag{2}$$

$$\text{where } H(t) = \chi\left(\left|F_{ex}(t)\right| - F_{\mu s}\right) + \left(1-\chi\left(\left|F_{ex}(t)\right| - F_{\mu s}\right)\right)\chi\left(\left|\dot{x}_1(t)\right| - \varepsilon_v\right). \tag{3}$$

$\chi(a) = \{1\ (a \geq 0), 0\ (a<0)\}$; and F_1 is the shear force applied to the sliding interface.

When a superstructure consisting of N-storeys is placed on the sliding mass, as shown in Figure 1(b), the equations of motion for both stick and slip states can be given as follows:

$$\begin{cases} m_{N+1}\ddot{y}_{N+1}(t) + f_{ckN+1}(t) = 0, \\ \vdots \\ m_2\ddot{y}_2(t) + f_{ck2}(t) - f_{ck3}(t) = 0, \\ F_1(t)\left(=\sum_{i=1}^{N+1} m_i\ddot{y}_i(t)\right) = F_{ex}(t)\left(1-H(t)\right) - F_{\mu v}(t)\operatorname{sgn}\left(\dot{x}_1(t)\right)H(t), \end{cases} \tag{4}$$

where $F_{ex}(t) = m_1\ddot{y}_g(t) + \sum_{i=2}^{N+1} m_i\ddot{y}_i(t)$, and $f_{cki}(= f_{ci} + f_{ki})$ is the resultant force of damping and restoring forces on the i^{th} storey $(i = 2, \ldots, N+1)$. Note that $F_{\mu v}(t) = F_{\mu s} = \mu_{\max}(\sum_{i=1}^{N+1} m_i)g$ when the kinematic friction $F_{\mu v}$ is equal to the maximum static friction $F_{\mu s}$. In addition, when the superstructure is a linear system with time-invariant damping and stiffness coefficients on the i^{th} storey, the resultant force becomes $f_{cki}(t)(= f_{ci}(t) + f_{ki}(t)) = c_i(\dot{y}_i(t) - \dot{y}_{i-1}(t)) + k_i(y_i(t) - y_{i-1}(t))$.

According to equations (2) and (4), the equation of motion for the sliding interface with and without the superstructure can be uniformly described by the following equation:

$$m_1\ddot{x}_1(t) = -\left(F_{ex}(t) + \operatorname{sgn}\left(\dot{x}_1(t)\right)\cdot F_{\mu v}(t)\right)\cdot H(t). \tag{5}$$

2.1.2. Shake Tables with Sliding Structures. The PID method is commonly employed in a shake table system as a basic controller acting on the table displacement. In most cases, the PID controller is designed such that the closed-loop

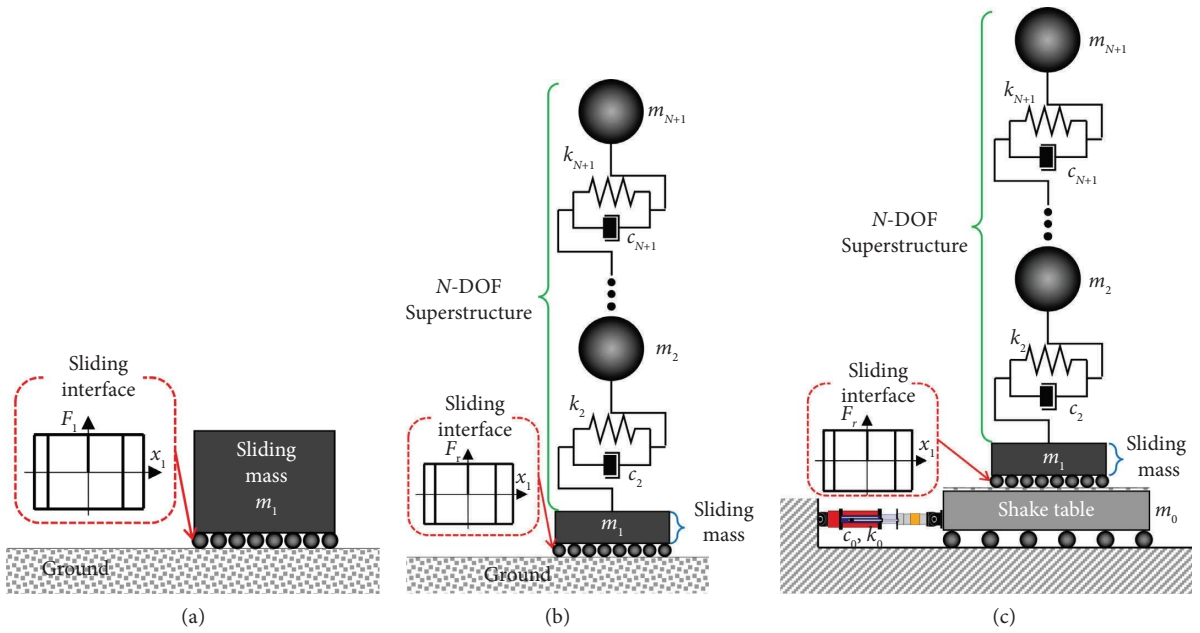

FIGURE 1: Sliding systems and a shake table: (a) sliding mass, (b) sliding structure on the ground, and (c) sliding structure placed on the table.

transfer function, including the table and the controller itself, has the following dynamics:

$$G_{0d}(s)\left(=G_{0/u}(s)\right)=\frac{y_0(s)}{u(s)}=\frac{\omega_{0b}^2}{s^2+2\zeta_{0b}\omega_{0b}s+\omega_{0b}^2}=\frac{k_{0b}}{m_{0b}s^2+c_{0b}s+k_{0b}}, \tag{6}$$

where s is the Laplace variable; y_0 is the table displacement; u is the control input signal, which has the dimension of displacement; and $\{m_{0b}, \omega_{0b}, \zeta_{0b}, c_{0b}, k_{0b}\}$ is the set of table mass, circular frequency, its corresponding damping ratio, and equivalent damping and stiffness coefficients, respectively, when no specimen is placed on the shake table. According to equation (6), the bare shake table in the time domain can be described by the following expression:

$$m_{0b}\ddot{y}_0(t)+c_{0b}\dot{y}_0(t)+k_{0b}y_0(t)=k_{0b}u(t). \tag{7}$$

when a sliding mass sustaining an N-DOF superstructure is placed on the table as a specimen, as shown in Figure 1(c), its equations of motion are given by the following equations:

$$\begin{cases} m_{N+1}\ddot{y}_{N+1}(t)+f_{ckN+1}(t)=0, \\ \vdots \\ m_2\ddot{y}_2(t)+f_{ck2}(t)-f_{ck3}(t)=0, \\ F_1(t)\left(=\sum_{i=1}^{N+1}m_i\ddot{y}_i(t)\right)=F_{ex}(t)(1-H(t))-F_{\mu v}(t)\mathrm{sgn}\left(\dot{x}_1(t)\right)H(t), \\ m_0\ddot{y}_0(t)+c_0\dot{y}_0(t)+k_0y_0(t)=k_0u(t)-F_1(t), \end{cases} \tag{8}$$

where $F_{ex}(t)=m_1\ddot{y}_0(t)+\sum_{i=2}^{N+1}m_i\ddot{y}_i(t)$; and $\{m_0, \omega_0, \zeta_0, c_0, k_0\}$ is the set of the table mass, circular frequency, its corresponding damping ratio, and equivalent damping and stiffness coefficients, respectively, when the specimen is placed on the table. Note that m_0 contains the bare table mass m_{0b} and the mass of some experimental rigs $m_{0\alpha}$.

According to equation (8), the shear force F_1, which is the friction force in the sliding interface, clearly disturbs the shake table. When the sliding structure has an interface with a near-zero friction coefficient, the friction force is negligible, and the sliding does not disturb the table control. However, when the force is not negligible owing to a high

friction coefficient, it disturbs the shake table control, resulting in control degradation. As F_1 in equation (8) is proportional to the mass of the sliding structure, the shake table control is considerably disturbed by the sliding of a heavy structure with a high friction coefficient. To properly excite a specimen on the table, the shake table must be accurately controlled, regardless of the properties of the specimen to be tested.

2.2. Nonlinear Signal-Based Control for a Shake Table Supporting a Sliding Structure. This study employed NSBC for shake table experiments with sliding structures and examined its control performance. Here, the principles of NSBC are briefly described and its controller design for table acceleration control is detailed.

2.2.1. NSBC for Acceleration Control at Shake Table Experiments. NSBC has the nonlinear signal feedback action as shown in Figure 2, as well as the feedforward controller derived from IBC, as shown in Figure 3. The nonlinear signal enables us to measure the unmodelled dynamics within the controlled system by comparing it with its linear model as follows:

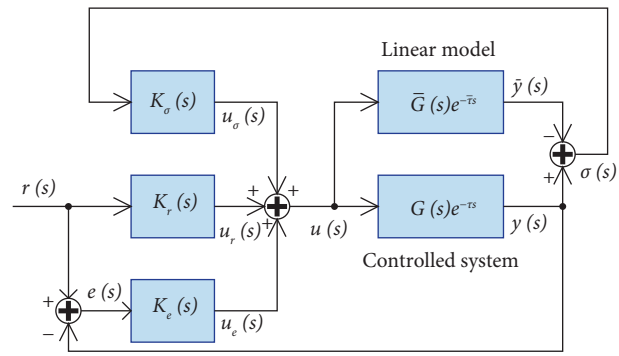

Figure 2: Nonlinear signal-based control.

$$\sigma(s)(=y(s)-\overline{y}(s))=\left(\overline{G}(s)e^{-\tau s}-\overline{G}(s)e^{-\overline{\tau}s}\right)u(s)=\Delta G_{\Delta\tau}(s)\overline{G}(s)e^{-\overline{\tau}s}u(s), \tag{9}$$

where $\Delta G_{\Delta\tau}(s)=(1+(\Delta G(s)/\overline{G}(s)))e^{-\Delta\tau s}-1$; σ is the nonlinear signal; y is the controlled output signal of the controlled system G; $\overline{y}$ is the output of the linear model $\overline{G}$; $\Delta G(=G-\overline{G})$ denotes the unmodelled dynamics, which are typically derived from some nonlinear characteristics within G; and $\Delta\tau(=\tau-\overline{\tau})$ is the difference between the pure time delay in the controlled system τ and its estimate $\overline{\tau}$. According to equation (9), the nonlinear signal at $\Delta\tau=0$ becomes $\sigma(s)=\Delta G(s)e^{-\overline{\tau}s}u(s)$. This indicates that, when the estimate of the pure time delay is accurate, the unmodelled dynamics, which cannot be directly measured, can be indirectly measured in the form of the nonlinear signal. Note that the description of the controlled system in NSBC (Figure 2) varies depending on the controlled output signal y: at displacement [acceleration] control, the controlled system is described by $G(s)=G_{0d}(s)(=y_0(s)/u(s))$ $[G(s)=G_{0a}(s)(=s^2G_{0d}(s))]$, and its linear model is $\overline{G}(s)=\overline{G}_{0d}(s)(=\overline{y}_0(s)/u(s))$ $[\overline{G}(s)=\overline{G}_{0a}(s)(=s^2\overline{G}_{0d}(s))]$.

Using the nonlinear signal, the error signal can be obtained as follows:

$$e(s)(=r(s)-y(s))=r(s)-\overline{y}(s)-\sigma(s)=r(s)-\overline{G}(s)e^{-\overline{\tau}s}u(s)-\sigma(s), \tag{10}$$

where e is the error signal; and r is the reference signal. As u in equation (10) is associated with the signals $\{r,e,\sigma\}$, the control input signal in NSBC is described as follows:

$$u(s)\left(=u_r(s)+u_e(s)+u_\sigma(s)\right)=K_r(s)r(s)+K_e(s)e(s)+K_\sigma(s)\sigma(s), \tag{11}$$

where $\{K_r,K_e,K_\sigma\}$ is the set of controllers acting on signals $\{r,e,\sigma\}$, respectively.

By substituting equation (11) into equation (10), the error signal can be rewritten as follows:

$$e(s)=\frac{1-\overline{G}(s)e^{-\overline{\tau}s}K_r(s)}{1+\overline{G}(s)e^{-\overline{\tau}s}K_e(s)}r(s)-\frac{1+\overline{G}(s)e^{-\overline{\tau}s}K_\sigma(s)}{1+\overline{G}(s)e^{-\overline{\tau}s}K_e(s)}\sigma(s). \tag{12}$$

The NSBC controllers in equation (11) are designed to realise a zero error in equation (12) with $\tau=\overline{\tau}=0$; this condition indicates cancelling the influence of the reference and nonlinear signals on the error signal. Then, the general forms of NSBC controllers are described by the following equation:

$$K_r(s)=\frac{F_r(s)}{\overline{G}(s)},K_e(s)=\frac{F_e(s)}{\overline{G}(s)},K_\sigma(s)=-\frac{F_\sigma(s)}{\overline{G}(s)}, \tag{13}$$

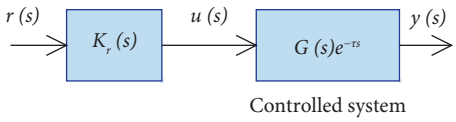

Figure 3: Inversion-based control: $K_r(s) = G(s)^{-1}$.

where $\{F_r, F_e, F_\sigma\}$ is the set of filters associated with the controllers $\{K_r, K_e, K_\sigma\}$, respectively. In equation (13), K_r is the feedforward controller based on the linear model transfer function $\overline{G}(s)$, and its sole use corresponds to IBC in Figure 3. K_σ is the nonlinear signal feedback controller used to cope with the unmodelled dynamics (e.g., nonlinear characteristics) within the controlled system. K_e is the error feedback controller optionally employed to forcibly minimise the error signal, which remains even after the activation of K_r and K_σ.

When NSBC was applied to shake table experiments with a steel structure [44], the controllers with $K_e(s) = 0$ accurately realised an earthquake excitation, even though the structure displayed significantly severe nonlinear characteristics. In the experiments, the following control input signal was found to be suitable for the acceleration control of a shake table:

$$u(s)\left(= u_r(s) + u_\sigma(s)\right) = K_r^* \ddot{r}(s) + K_\sigma^*(s)\ddot{\sigma}(s), \tag{14}$$

where $\ddot{\sigma}(s) = \ddot{y}_0(s) - \ddot{\overline{y}}_0(s)$; $\ddot{r}$ is the reference acceleration signal to be realised on the table; $\ddot{y}_0$ is the shake table acceleration signal measured by a sensor, and $\ddot{\overline{y}}_0$ is the acceleration signal computationally calculated using $\overline{G}_{0a}$ and u. In equation (14), the signal u_σ, which relies on the feedback signal $\ddot{\sigma}$, drives to cancel the influence of the nonlinear signal on the error signal e, resulting in a high control accuracy. When the linear model transfer function for the table acceleration and control input signal, $\overline{G}_{0a}(s)$, is given, it can be employed as $\overline{G}(s) = \overline{G}_{0a}(s)$ in Figure 2. When the inversion of $\overline{G}_{0a}(s)$ is a stable and proper transfer function, the controllers in equation (14) become

$$K_r^*(s) = \frac{1}{\overline{G}_{0a}(s)}, K_\sigma^*(s) = -\frac{F_\sigma(s)}{\overline{G}_{0a}(s)}. \tag{15}$$

The filter F_σ basically limits the frequency components from being fed back, and its design affects the stability. A previous study [44] on the stability of NSBC demonstrated that the second-order bandpass Butterworth filter passing the range of 0.2–20.0 Hz could effectively maintain stability in shake table experiments with nonlinear characteristics. Thus, this study also employed the same bandpass filter as F_σ. This bandpass range sufficiently covers the frequency range of typical seismic acceleration records.

2.2.2. Stability of NSBC. The stability of NSBC depends on the feedback signals, e and σ, which are uniformly expressed by the following equation:

$$\begin{bmatrix} e(s) \\ \sigma(s) \end{bmatrix} = \frac{1}{L(s)} \begin{bmatrix} 1 - \left(K_r(s) + K_\sigma(s)\right)\Delta G_{\Delta\tau}(s)\overline{G}(s)e^{-\overline{\tau}s} - K_r(s)\overline{G}(s)e^{-\overline{\tau}s} \\ \left(K_r(s) + K_e(s)\right)\Delta G_{\Delta\tau}(s)\overline{G}(s)e^{-\overline{\tau}s} \end{bmatrix} r(s), \tag{16}$$

where

$$L(s) = 1 + \left[\left(\Delta G_{\Delta\tau}(s) + 1\right)\overline{G}(s)K_e(s) - \Delta G_{\Delta\tau}(s)\overline{G}(s)K_\sigma(s)\right]e^{-\overline{\tau}s}, \tag{17}$$

which is the closed-loop characteristic equation governing the stability.

According to equation (16), the error signal e has the following relation with the reference signal r:

$$G_{e/r}(s)\left(= \frac{e(s)}{r(s)}\right) = \frac{1 - \left\{\left(K_r(s) + K_\sigma(s)\right)\Delta G_{\Delta\tau}(s) + K_r(s)\right\}\overline{G}(s)e^{-\overline{\tau}s}}{L(s)}. \tag{18}$$

Equation (18) can be assessed for various controller designs, once the controlled system with nonlinear characteristics is equivalently or approximately described by a Laplace form.

Stability of NSBC with the controller designs can be assessed on the basis of equation (17). When the error feedback action is not activated, i.e., $K_e(s) = 0$, which is the case in this study, it becomes

$$\begin{aligned} L(s) &= 1 - \Delta G_{\Delta\tau}(s)\overline{G}(s)K_\sigma(s)e^{-\overline{\tau}s} \\ &= 1 + \Delta G_{\Delta\tau}(s)F_\sigma(s)e^{-\overline{\tau}s}. \end{aligned} \tag{19}$$

According to equation (19), the linear model $\overline{G}$ and filter $F_\sigma(s)$ can be used for maintaining stability and increasing stability margins, as they are factors that are flexibly designed in the equation.

2.2.3. Linear Model and Controller Designs for Shake Table Experiments with Sliding Structures. A linear model of the controlled system plays a fundamental role in NSBC. This study introduces a linear model design based on the stick state of the sliding structure because the structure remains within the state in a system identification test, which are commonly performed before the main experiments using earthquake excitations. This design is exemplified for a shake table sustaining a sliding structure shown in Figure 1(c).

Based on the stick state of the sliding structure, a linear model for the shake table and sliding structure can be described as follows:

$$\begin{cases} \overline{m}_{N+1}\ddot{\overline{y}}_{N+1}(t) + \overline{f}_{ckN+1}(t) = 0, \\ \quad\vdots \\ \overline{m}_2\ddot{\overline{y}}_2(t) + \overline{f}_{ck2}(t) - \overline{f}_{ck3}(t) = 0, \\ \ddot{\overline{y}}_1(t) = \ddot{\overline{y}}_0(t), \\ \overline{m}_0\ddot{\overline{y}}_0(t) + \overline{c}_0\dot{\overline{y}}_0(t) + \overline{c}_0\overline{y}_0(t) - \overline{f}_{ck2}(t) = \overline{k}_0 u(t) - \overline{m}_1\ddot{\overline{y}}_1(t), \end{cases} \tag{20}$$

where $\overline{f}_{cki}(t)(=\overline{f}_{ci}(t)+\overline{f}_{ki}(t)) = \overline{c}_i(\dot{\overline{y}}_i(t) - \dot{\overline{y}}_{i-1}(t)) + \overline{k}_i(\overline{y}_i(t) - \overline{y}_{i-1}(t))$; $\left\{\overline{y}_i, \overline{m}_i, \overline{c}_i, \overline{k}_i, (i = 1\cdots N+1)\right\}$ denotes the displacement, mass, damping coefficient, and stiffness in the i^{th} storey of the linear model, respectively; and $\left\{\overline{y}_0, \overline{m}_0, \overline{c}_0, \overline{k}_0\right\}$ is the set denoting the displacement, mass, damping coefficient, and stiffness associated with the shake table part in the linear model, respectively.

This linear model can be described by the set of transfer functions for the corresponding stories, which is described as follows:

$$\begin{cases} \overline{G}_{N+1/N}(s)\left(=\dfrac{\overline{y}_{N+1}(s)}{\overline{y}_N(s)}\right) = \dfrac{\overline{c}_{N+1}s + \overline{k}_{N+1}}{\overline{m}_{N+1}s^2 + \overline{c}_{N+1}s + \overline{k}_{N+1}}, \\ \overline{G}_{N/N-1}(s)\left(=\dfrac{\overline{y}_N(s)}{\overline{y}_{N-1}(s)}\right) = \dfrac{\overline{c}_N s + \overline{k}_N}{\left(\overline{m}_N s^2 + (\overline{c}_{N+1} + \overline{c}_N)s + \overline{k}_{N+1} + \overline{k}_N\right) - \left(\overline{c}_{N+1}s + \overline{k}_{N+1}\right)\overline{G}_{N+1/N}(s)}, \\ \quad\vdots \\ \overline{G}_{2/1}(s)\left(=\dfrac{\overline{y}_2(s)}{\overline{y}_1(s)}\right) = \dfrac{\overline{c}_2 s + \overline{k}_2}{\overline{m}_2 s^2 + (\overline{c}_3 + \overline{c}_2)s + \overline{k}_3 + \overline{k}_2 - \left(\overline{c}_3 s + \overline{k}_3\right)\overline{G}_{3/2}(s)}, \\ \overline{G}_{1/0}(s)\left(=\dfrac{\overline{y}_1(s)}{\overline{y}_0(s)}\right) = 1, \\ \overline{G}_{0/u}(s)\left(=\dfrac{\overline{y}_0(s)}{u(s)}\right) = \dfrac{\overline{k}_0}{(\overline{m}_0 + \overline{m}_1)s^2 + (\overline{c}_0 + \overline{c}_2)s + \overline{k}_0 + \overline{k}_2 - \left(\overline{c}_2 s + \overline{k}_2\right)\overline{G}_{2/1}(s)}. \end{cases} \tag{21}$$

In equation (21), the transfer function $\overline{G}_{i/i-1}(s)$ contains $\overline{G}_{i+1/i}(s)$, which also contains $\overline{G}_{i+2/i+1}(s)$, and this relation continues until $i = N$. Thus, the transfer function $\overline{G}_{0/u}(s)$ is obtained by calculating the transfer functions in the order of $\overline{G}_{N+1/N}(s), \overline{G}_{N/N-1}(s), \cdots, \overline{G}_{1/0}(s), \overline{G}_{0/u}(s)$. As $\overline{G}_{0/u}(s)$ denotes the relation between the table displacement and the control input signal, it can be expressed by $\overline{G}_{0d}(s) = \overline{G}_{0/u}(s)$ and its relation with the table acceleration becomes $\overline{G}_{0a}(s) = s^2\overline{G}_{0d}(s)$. By employing $\overline{G}_{0a}(s)$ as $\overline{G}(s)$ in Figure 2, equation (14) can be used to determine the input signal for table acceleration control using the controller in equation (15).

The design of the linear model is fairly flexible, allowing various settings for the linear model parameters: $\left\{\overline{m}_i, \overline{c}_i, \overline{k}_i, (i = 1\cdots N+1)\right\}$ and $\left\{\overline{m}_0, \overline{c}_0, \overline{k}_0\right\}$ in this case. In fact, NSBC achieved perfect tracking control of multi-storey

nonlinear systems even by a linear model whose stiffness coefficients are intentionally set to zero, despite the presence of stiffness elements in the actual controlled system [45]. In addition, a linear model with a larger damping than the actual control system enhances the stability margin for nonlinear system control. Based on these features, a linear model for NSBC can be flexibly designed to enhance its performance.

3. Numerical Examination

3.1. Numerical Conditions. A series of shake table experiments in the numerical simulation was performed using the setup in Figure 4(a), with the setting of a constant damping coefficient and a trilinear hysteretic spring shown in Figure 4(b) within the SDOF superstructure. An excitation employed for the simulation is the acceleration data shown in Figure 5, which was recorded by the Japan Meteorological Agency (JMA) during the Hyogo-Ken Nanbu (Kobe) earthquake in 1995. These data are used as the reference signal to be reproduced in the shake table experiments and referred to as the JMA Kobe motion in this study.

3.1.1. Shake Table and Sliding Structure. The equations of motion for the table an sliding structure in Figure 4(a) are as follows:

$$\begin{cases} m_2\ddot{y}_2(t) + c_2\left(\dot{y}_2(t) - \dot{y}_1(t)\right) + f_{k2}(t) = 0, \\ F_1(t)\left(= m_1\ddot{y}_1(t) + m_2\ddot{y}_2(t)\right) = F_{ex}(t)\left(1 - H(t)\right) - F_{\mu v}(t)\mathrm{sgn}\left(\dot{x}_1(t)\right)H(t), \\ m_0\ddot{y}_0(t) + c_0\dot{y}_0(t) + k_0 y_0(t) = k_0 u(t) - F_1(t), \end{cases} \tag{22}$$

where $F_{ex}(t) = m_1\ddot{y}_0(t) + m_2\ddot{y}_2(t)$. The restoring force f_{k2}, derived from the nonlinear spring with the characteristic shown in Figure 4(b), is described as follows:

$$f_{k2}(t) = r_{22}k_2\delta_2(t) + \left(1 - r_{21}\right)k_2 z_{21}(t) + \left(r_{21} - r_{22}\right)k_2 z_{22}(t), \tag{23}$$

where $\delta_2(t) = y_2(t) - y_1(t)$; $\dot{z}_{2l}(t) = \dot{\delta}_2(t)\{\chi(\dot{\delta}_2(t))\chi(\Delta_{2l} - z_{2l}(t)) + \chi(-\dot{\delta}_2(t))\chi(\Delta_{2l} + z_{2l}(t))\}$ $(l = 1,2)$; and $\{\Delta_{2l}, r_{2l}\}$ is the set of the l^{th} elastic limit and stiffness reduction factor of the nonlinear spring, respectively.

As kinematic friction is generally affected by the sliding velocity [53, 61, 64, 69], this study reflects its characteristics in numerical simulations. The kinematic friction in equation (22) can be expressed as follows:

$$F_{\mu v}(t) = \left\{\mu_{\min} + \left(\mu_{\max} - \mu_{\min}\right)e^{-\gamma\left|\dot{x}_1(t)\right|}\right\}\left(m_1 + m_2\right)g, \tag{24}$$

where $\mu_{\min}$ is the minimum friction coefficient during sliding and γ is the intensity of the friction reduction. Note that equation (24) with $\gamma = 0.0$ maintains the maximum static friction during the sliding state.

The detailed parameters employed in the simulation were based on a system identification test performed on an actual shake table sustaining a sliding steel structure, which is shown later in Section 4.1. Then, the parameters of the shake table were set as follows: $m_0\,(= m_{0b} + m_{0\alpha} = 200 + 115\,\text{kg}) = 315\,\text{kg}$, $c_0 = 4.78\,\text{kNs/m}$, and $k_0 = 71.06\,\text{kN/m}$. The sliding structure was designed to have a sliding mass of $m_1 = 225\,\text{kg}$ and an SDOF superstructure with the following parameters: $m_2 = 200\,\text{kg}$, $c_2 = 120\,\text{Ns/m}$, and $k_2 = 43.00\,\text{kN/m}$. The trilinear hysteretic spring in equation (23) was modelled with $\Delta_{21} = 0.03\,\text{m}$, $\Delta_{22} = 1.5\,\text{kNs/m}\Delta_{21}$, $r_{21} = 0.5$, and $r_{22} = 0.05$. The kinematic friction in equation (24) was modelled as $\mu_{\max} = 0.22$, $\mu_{\min} = 0.15$, and $\gamma = 20.0$, according to a previous study on graphite lubrication of steel and mortar [64]. The velocity limit for the Karnopp model used in equation (22) was set to $\varepsilon_v = 0.001$, which is commonly used in this model [68]. The pure time delay was set as $\tau = 4.0\,\text{ms}$, according to the identification test.

Prior to studying the interaction between a shake table and sliding structure, the structure with the aforementioned parameters was numerically placed on the ground and simulated with 80% JMA Kobe motion. The response of the structure is shown in Figure 6, including the friction varying with the sliding velocity. By comparing with the structural response of the sliding mass rigidly fixed on the ground, as shown in Figure 6(c), it can be easily observed that the occurrence of sliding effectively mitigates the structural damage and contributes to maintaining the structure almost within the elastic range. The numerical simulations for shake table experiments with a sliding structure are expected to produce identical or sufficiently similar results.

3.1.2. Control Accuracy. This study evaluated the control accuracy of a shake table experiment, based on the similarity of the realised table acceleration and its reference acceleration signal. The similarities in the time and frequency domains were calculated by using the following eqaution:

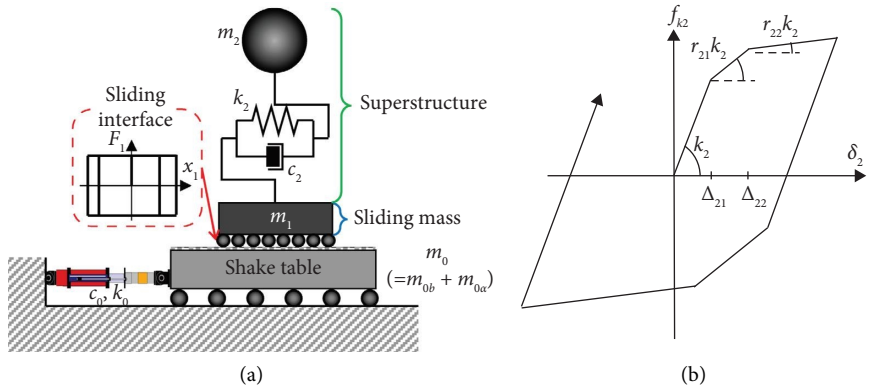

FIGURE 4: Shake table experiment with a sliding mass and an SDOF superstructure: (a) schematic drawing and (b) trilinear hysteretic spring embedded in the superstructure.

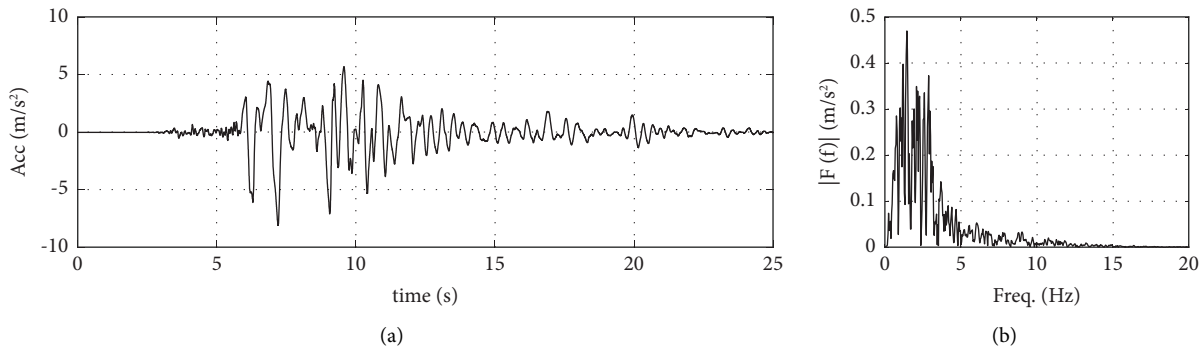

FIGURE 5: JMA Kobe motion: (a) time history acceleration and (b) Fourier amplitude spectra.

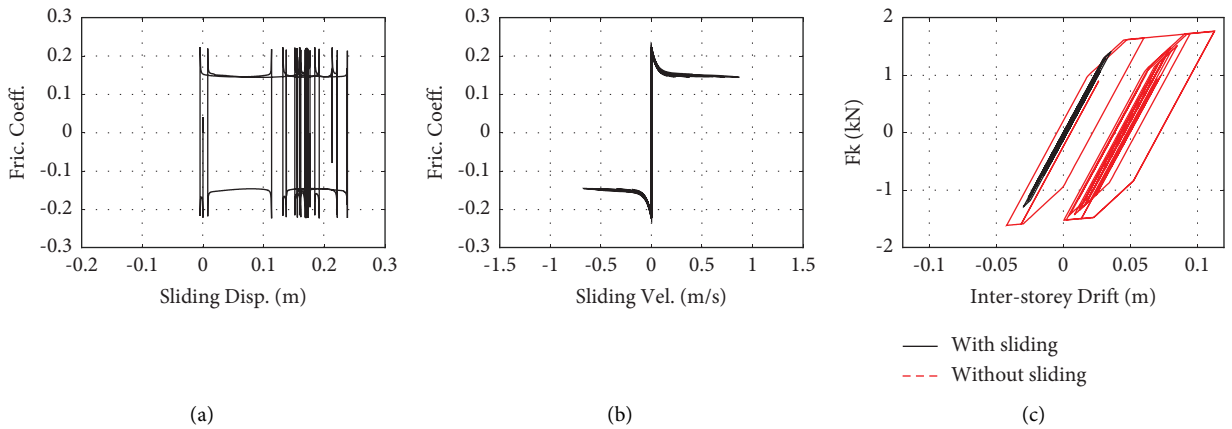

FIGURE 6: Responses of a sliding structure subjected to 80% JMA Kobe motion: (a) friction coefficient vs. sliding displacement, (b) friction coefficient vs. sliding velocity, and (c) hysteresis in the superstructure.

$$S_t(\ddot{r}, \ddot{y}_0) = \left(1 + \frac{\sum(\ddot{r}(t) - \ddot{y}_0(t))^2}{\sum \ddot{r}(t)^2}\right)^{-1} \times 100\%,$$

$$S_f(\ddot{r}, \ddot{y}_0) = \left(1 + \frac{\sum(A_r(f) - A_{y0}(f))^2}{\sum A_r(f)^2}\right)^{-1} \times 100\%, \quad (25)$$

where $\{A_r, A_{y0}\}$ is the set of Fourier amplitude spectra of $\{\ddot{r}, \ddot{y}_0\}$, respectively. S_t directly measures the similarity of the two signals from the time history data, while S_f is focussed on the amplitudes of the Fourier spectra in a limited frequency range. S_f in this study is evaluated in the range of 0.1–20.0 Hz, which covers the frequency components in most earthquake excitations.

Table 1: Numerical results of IBC with Linear Model 1.

Excitation	JMA Kobe					
Amplitude	10%	20%	40%	60%	80%	100%
$S_f[\ddot{r}, \ddot{y}_0]$ (%)	99.41	81.07	37.91	26.08	21.04	18.62
$S_t[\ddot{r}, \ddot{y}_0]$ (%)	95.86	67.51	29.74	20.67	16.95	15.13

3.2. Numerical Simulation. The linear model required for NSBC was built based on the stick state of a sliding structure, and its equations of motion can be described by equation (20) with $N = 1$. Based on equation (21) with $N = 1$, the transfer functions for the linear model can be obtained as follows:

$$\begin{cases} \overline{G}_{2/1}(s)\left(=\dfrac{\overline{y}_2(s)}{\overline{y}_1(s)}\right) = \dfrac{\overline{c}_2 s + \overline{k}_2}{\overline{m}_2 s^2 + \overline{c}_2 s + \overline{k}_2}, \\ \overline{G}_{0/u}(s)\left(=\dfrac{\overline{y}_0(s)}{u(s)}\right) = \dfrac{\overline{k}_0}{(\overline{m}_0 + \overline{m}_1)s^2 + (\overline{c}_0 + \overline{c}_2)s + \overline{k}_0 + \overline{k}_2 - (\overline{c}_2 s + \overline{k}_2)\overline{G}_{2/1}(s)}, \\ \overline{G}_{0a}(s)\left(=\dfrac{s^2\overline{y}_0(s)}{u(s)}\right) = s^2\overline{G}_{0/u}(s). \end{cases} \tag{26}$$

By employing the linear model as $\overline{G}(s) = \overline{G}_{0a}(s)$ in Figure 2, the NSBC input signal for Figure 4 is determined using equations (14) and (15). The filter F_σ was designed as a second-order Butterworth filter with a bandpass range of 0.2–20 Hz.

The parameters in the linear model were designed using the initial parameters of the controlled system, $\{\overline{m}_0, \overline{c}_0, \overline{k}_0, \overline{m}_1, \overline{m}_2, \overline{c}_2, \overline{k}_2\} = \{m_0, c_0, k_0, m_1, m_2, c_2, k_2\}$ and $\overline{\tau} = \tau$. This design is equivalent to the case where all initial parameters of the controlled system (i.e., the shake table and sliding structure) are known and reflected in the NSBC controllers, and it is referred to as Linear Model 1 in this study. In the simulation, the unmodelled dynamics is the nonlinearity within the superstructure only, and the shake table does not have any nonlinear characteristics, although actual systems in practice do. Noise was added intentionally to the table acceleration and displacement to make the simulation more realistic.

3.2.1. Numerical Results of IBC. Prior to examining NSBC, shake table experiments were computationally simulated with IBC, which was executed in the form of NSBC with $K_e(s) = K_\sigma(s) = 0$. The simulations were performed for JMA Kobe motion with different amplitudes: {10%, 20%, 40%, 60%, 80%, and 100%}. The results are summarised in Table 1. The detailed results for 20% and 80% amplitudes are illustrated in Figures 7 and 8, respectively. These two amplitudes were selected to maintain the consistency with the experimental results shown later.

According to Table 1, the control accuracy for the 10% excitation is satisfactory, especially in S_f. This is because a nonlinear characteristic does not appear under the excitation owing to the small amplitude, which is not sufficiently large to induce sliding in the structure. As shown in Figure 7, the structure under 20% excitation clearly slid. The sliding has degraded the table control of IBC, resulting in a significant reduction from the results of the 10% excitation, as shown in Table 1.

The control accuracies decreased significantly at larger excitations, as shown in Table 1. At 80% excitation, the realised table acceleration significantly differed from the reference signal in time and frequency domains, as shown in Figure 8, resulting in extremely low accuracies: $S_f = 21.04\%$ and $S_t = 16.95\%$. This result indicates that the expected experiment shown in Figure 6 is impossible using IBC. The results of 100% excitation were even worse than those of the 80% excitation. These results clarify the ineffectiveness of IBC for shake table experiments with a sliding structure.

3.2.2. Numerical Results of NSBC. Shake table experiments based on NSBC with Linear Model 1 were computationally simulated for the JMA Kobe motion with the same amplitudes as those conducted with IBC. The results are summarised in Table 2, and the detailed results of 20% and 80% excitations are illustrated in Figures 9 and 10, respectively.

As shown in Figure 9, NSBC has accurately realised 20% JMA Kobe motion, even though the structure has clearly slid on the table. This resulted in satisfactory accuracies: $S_f = 99.13\%$ and $S_t = 95.73\%$, which are considerably better than those of IBC, which are shown in Table 1. As shown in Table 2, at even larger excitations, NSBC produced similar or better results than those at 20% excitation. At 80% excitation, the table acceleration realised by NSBC was satisfactorily similar to the reference signal in the time and frequency domains, as observed in Figure 10. In addition, the experiment realised

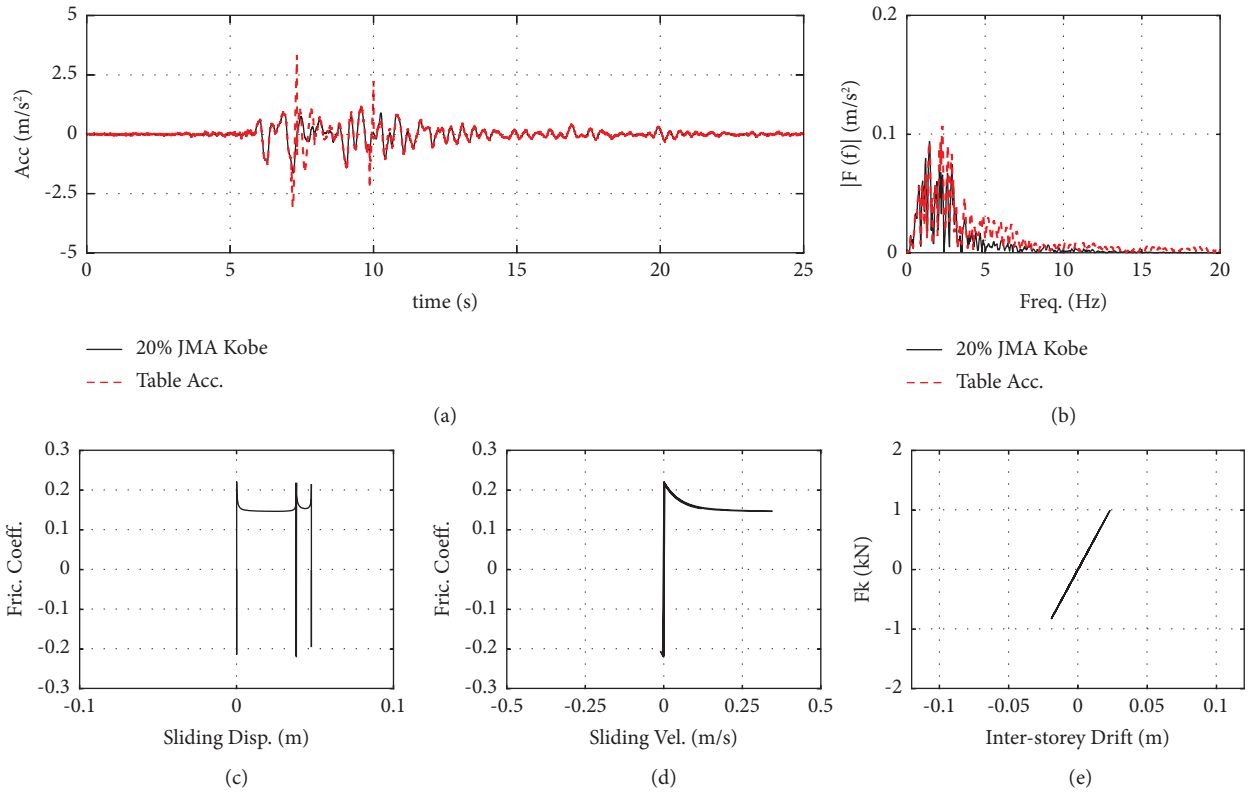

FIGURE 7: Numerical results of IBC for 20% JMA Kobe motion: (a) time history of the table acceleration, (b) Fourier amplitude spectra of the table acceleration, (c) friction coefficient vs. sliding displacement, (d) friction coefficient vs. sliding velocity, and (e) shear force vs. inter-storey drift in the superstructure.

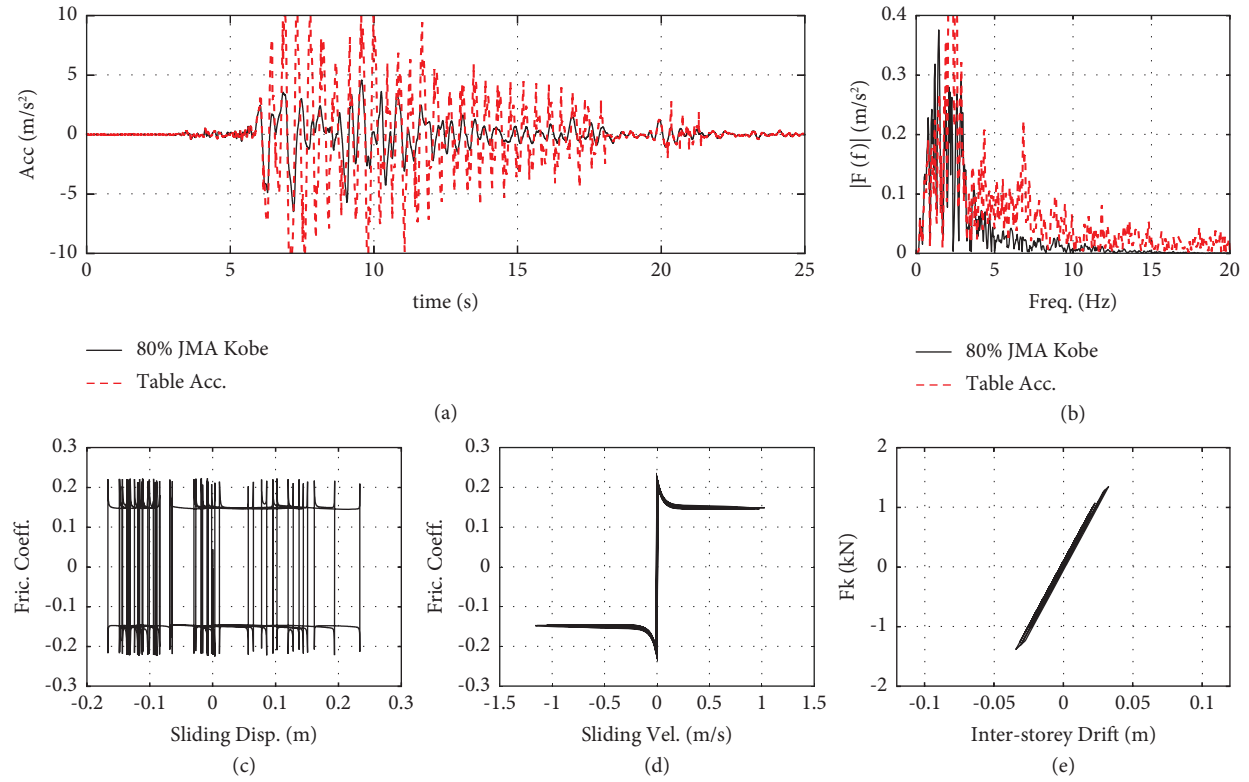

FIGURE 8: Numerical results of IBC for 80% JMA Kobe motion: (a) time history of the table acceleration, (b) Fourier amplitude spectra of the table acceleration, (c) friction coefficient vs. sliding displacement, (d) friction coefficient vs. sliding velocity, and (e) shear force vs. inter-storey drift in the superstructure.

Table 2: Numerical results of NSBC with Linear Model 1.

Excitation	JMA Kobe					
Amplitude	10%	20%	40%	60%	80%	100%
$S_f[\ddot{r}, \ddot{y}_0]$ (%)	99.73	99.13	98.61	98.84	98.80	99.03
$S_t[\ddot{r}, \ddot{y}_0]$ (%)	94.99	95.73	95.44	96.38	96.46	96.84

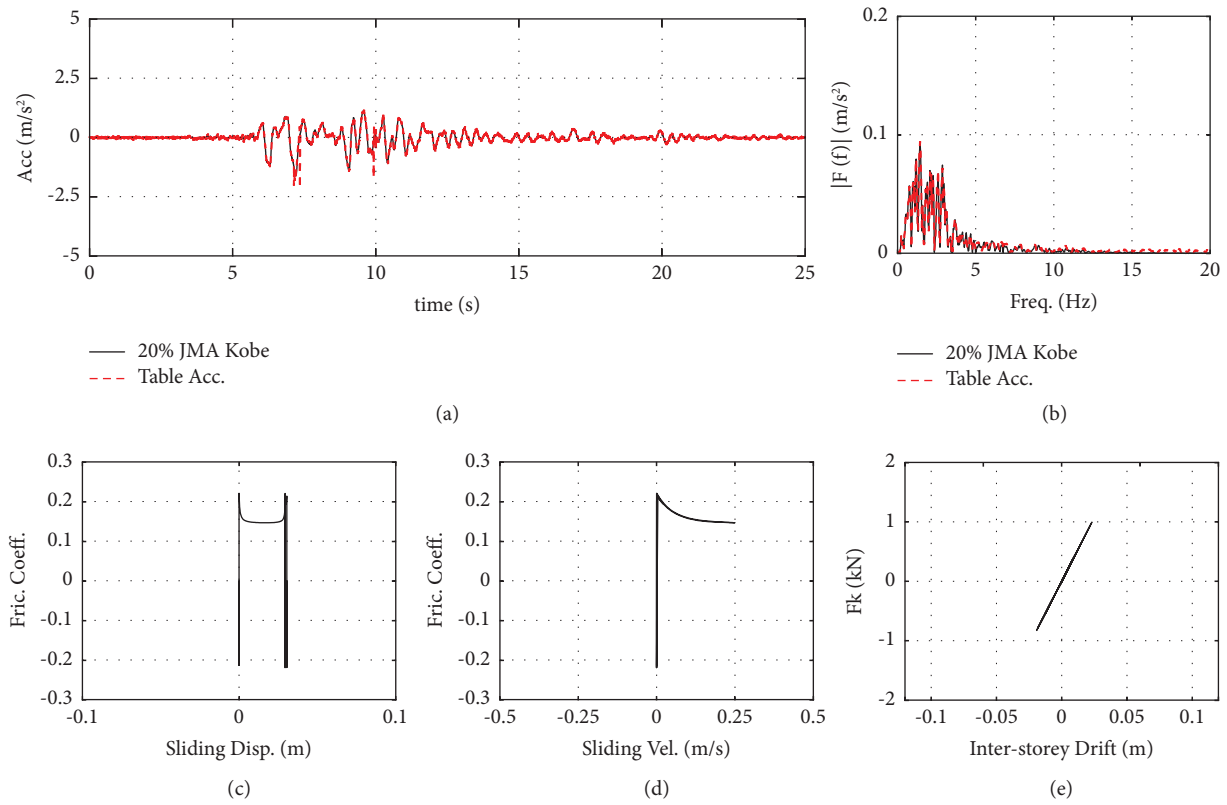

Figure 9: Numerical results of NSBC for 20% JMA Kobe motion: (a) time history of the table acceleration, (b) Fourier amplitude spectra of the table acceleration, (c) friction coefficient vs. sliding displacement, (d) friction coefficient vs. sliding velocity, and (e) shear force vs. inter-storey drift in the superstructure.

by NSBC was sufficiently close to the expected experiment shown in Figure 6. Even at 100% excitation, NSBC did not exhibit control degradation, as observed in Table 2, confirming its effectiveness in shake table experiments with a sliding structure. Note that S_t in Table 2 is improved at larger excitations because noise in the table acceleration becomes less influential to the index as the amplitude increases.

3.3. Stability Margin and Its Improvement by Linear Model Designs. NSBC with Linear Model 1 can effectively control a shake table sustaining a sliding structure, according to Section 3.2.2. However, stability is not guaranteed during the actual practice because the numerical simulations were performed without uncertainty within shake tables, which are typically observed during actual practices. To assess the stability and improve its margin, we introduce a stability analysis of NSBC for shake table control with a sliding structure and a linear model design in which linear model parameters are intentionally tuned to increase the stability margin. As a new design, Linear Model 1.5 is built by using $\overline{G}_{0a}(s)$ in equation (26) with the parameters, $\{\overline{m}_0, \overline{c}_0, \overline{k}_0, \overline{m}_1, \overline{m}_2, \overline{c}_2, \overline{k}_2\} = \{m_0, 1.5c_0, 1.5k_0, m_1, m_2, c_2, k_2\}$.

The stability analysis conducted in this study is based on table dynamics during two states (stick and slip) of the structure on the table. As the linear model is built based on the dynamics during the stick state, as shown in equation (26), the controlled system needs to be represented by the dynamics during the slip state. However, as sliding is a nonlinear phenomenon, it cannot be precisely described by a Laplace transform. Thus, by disregarding the influence of the sliding structure and friction, this study describes the controlled system as follows:

$$G_{0a}(s)\left(=\frac{s^2 y_0(s)}{u(s)}\right)=\frac{k_0 s^2}{m_0 s^2+c_0 s+k_0}. \tag{27}$$

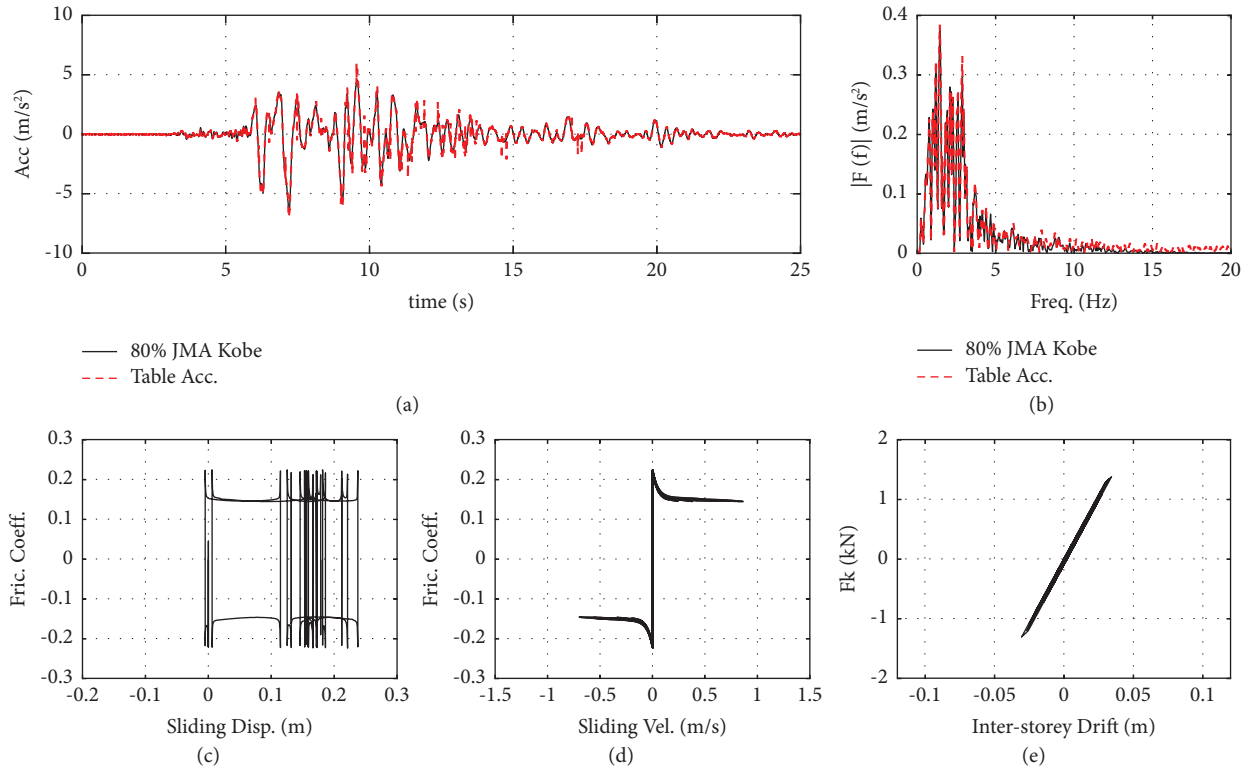

FIGURE 10: Numerical results of NSBC for 80% JMA Kobe motion: (a) time history of the table acceleration, (b) Fourier amplitude spectra of the table acceleration, (c) friction coefficient vs. sliding displacement, (d) friction coefficient vs. sliding velocity, and (e) shear force vs. inter-storey drift in the superstructure.

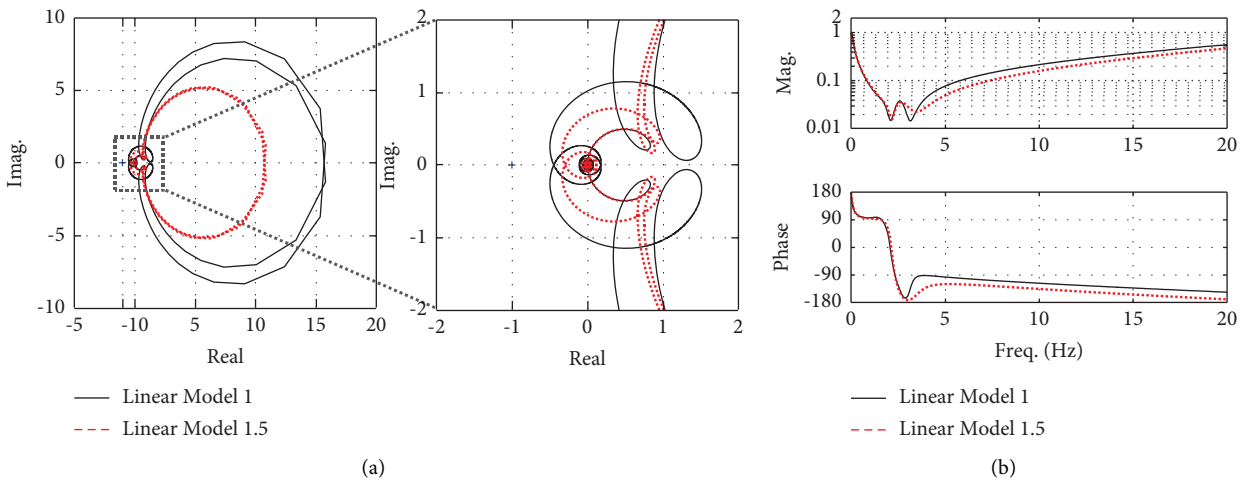

FIGURE 11: Stability and error of NSBC with different linear models: (a) Nyquist curves and (b) $G_{e/r}(s)$.

The modelling error dynamics ΔG, which is necessary for the stability analysis based on equation (19), can be approximated by the set of $G(s) = G_{0a}(s)$ in equation (27) and $\overline{G}(s) = \overline{G}_{0a}(s)$ in equation (26).

Stability of NSBC based on Linear Models 1 and 1.5 was analysed, and the results are illustrated in Figure 11 along with the relevant error. According to Figure 11(a), the stability margin of Linear Model 1.5 is greater than that of Linear Model 1, indicating the effectiveness of the design. In Figure 11(b), the error dynamics of Linear Model 1.5 are not significantly different from those of Linear Model 1.

Simulations with the numerical conditions identical to those described in Section 3.2 were performed with NSBC based on Linear Model 1.5, and the results are summarised in Table 3.

Table 3: Numerical results of NSBC with Linear Model 1.5

Excitation	JMA Kobe					
Amplitude	10%	20%	40%	60%	80%	100%
$S_f[\ddot{r}, \ddot{y}_0]$ (%)	99.58	98.69	97.53	97.95	97.97	98.23
$S_t[\ddot{r}, \ddot{y}_0]$ (%)	94.82	95.14	94.13	95.05	95.19	95.70

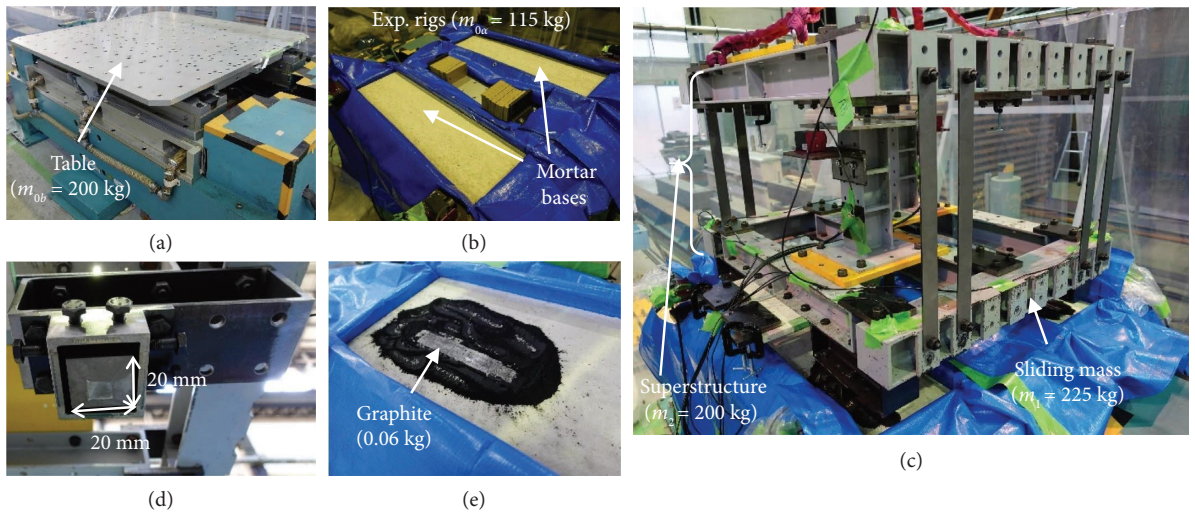

Figure 12: Experimental setup: (a) bare shake table, (b) mortar bases, (c) iron block, (d) lubrication by graphite, and (e) sliding structure (SDOF structure and sliding mass) on the table.

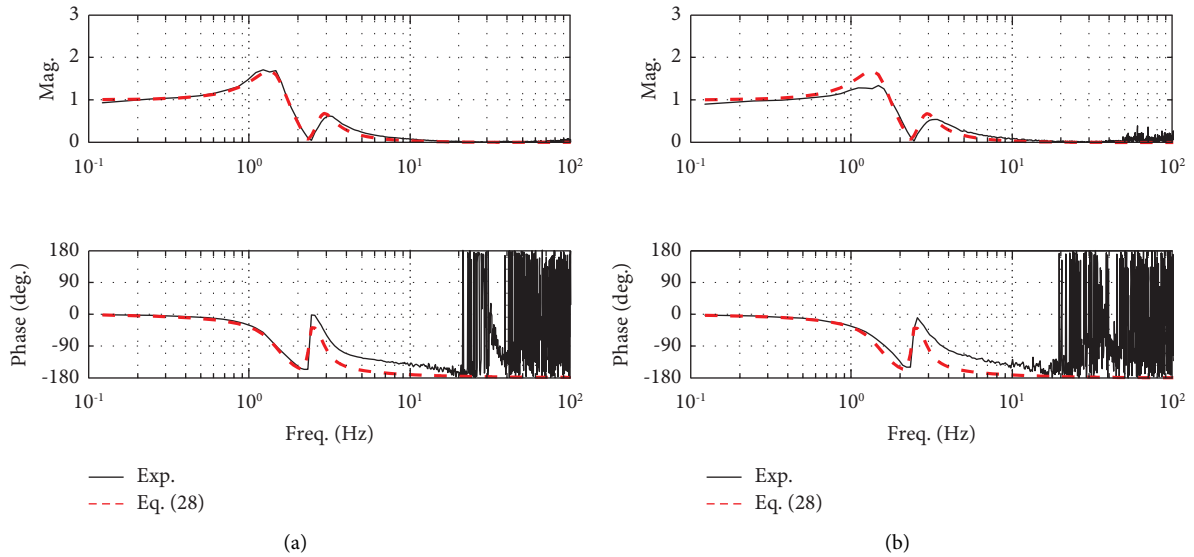

Figure 13: Table dynamics, G_{0d}, identified by band limited white-noise random excitation with different amplitudes: (a) 10.0 mm and (b) 2.0 mm.

Table 4: Experimental results of IBC based on Linear Model 1.

Excitation	JMA Kobe	
Amplitude	10%	20%
$S_f[\ddot{r}, \ddot{y}_0]$ (%)	94.10	79.43
$S_t[\ddot{r}, \ddot{y}_0]$ (%)	81.82	61.65

Linear Model 1.5 also achieved the satisfactory control accuracies, as shown in in Table 3, although the results are slightly lower than those of Linear Model 1, as shown in Table 2. This result indicates that Linear Model 1.5 attains a higher stability margin than Linear Model 1, achieving similar high control performance.

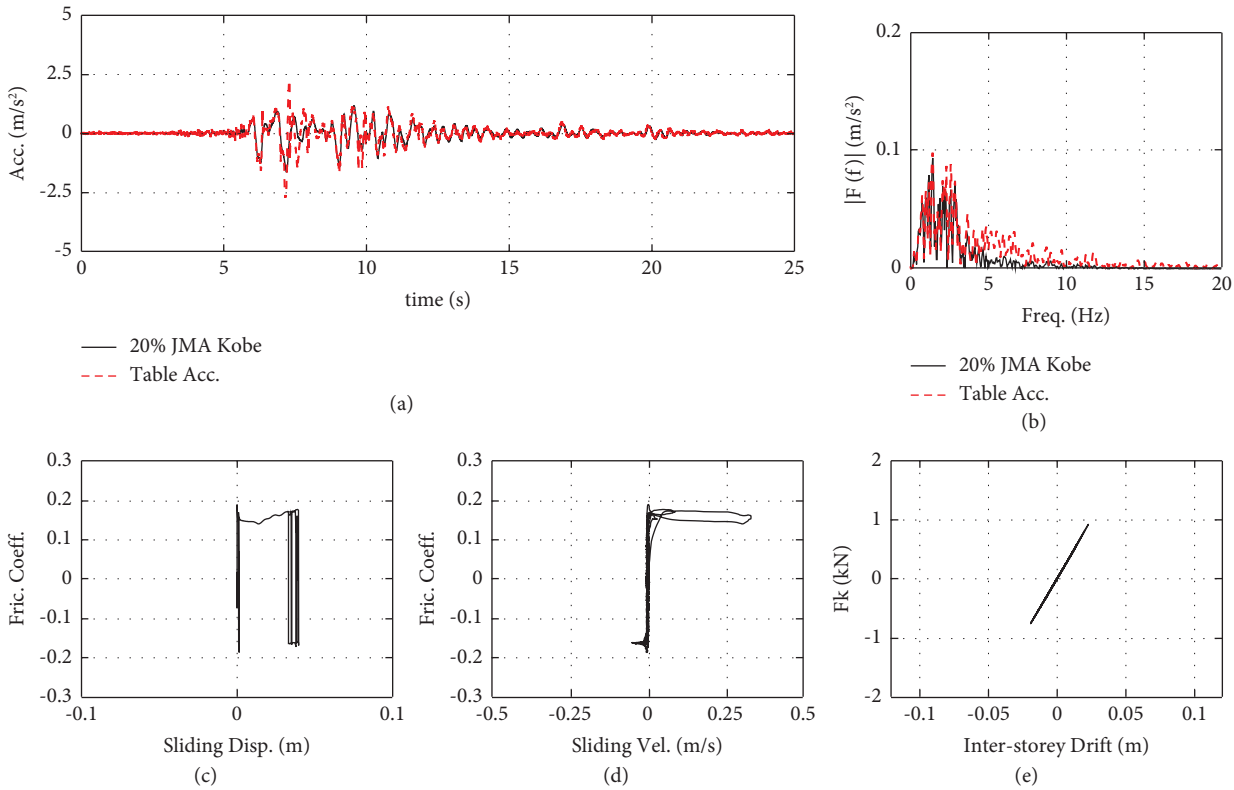

FIGURE 14: Experimental results of IBC based on Linear Model 1 for 20% JMA Kobe motion: (a) time history of the table acceleration, (b) Fourier amplitude spectra of the table acceleration, (c) friction coefficient vs. sliding displacement, (d) friction coefficient vs. sliding velocity, and (e) shear force vs. inter-storey drift in the superstructure.

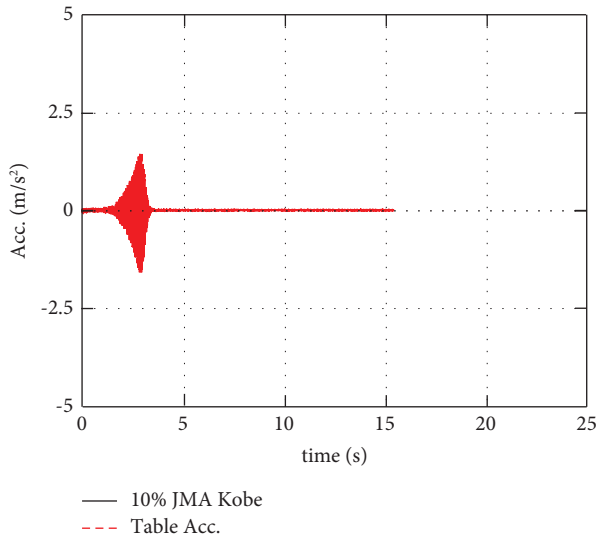

FIGURE 15: Experimental results of NSBC based on Linear Model 1 for 10% JMA Kobe motion: time history of table acceleration.

4. Experimental Examination

4.1. Experimental Conditions, System Identification, and Linear Models. Shake table experiments in this study were performed using a single-axis electrodynamic table, shown in Figure 12(a), which has a size of 1.2×1.2 m and a weight of 200 kg. A set of mortar bases, shown in Figure 12(b), was placed on the table, and a sliding steel structure was placed on the mortar bases, as shown in Figure 12(c). This steel structure consisted of two masses connected by steel plates. The first mass corresponds to the sliding mass in Figure 4(a), and the second mass and plates correspond to the superstructure in

Table 5: Experimental results of NSBC based on Linear Model 1.5.

Excitation	JMA Kobe				
Amplitude	10%	20%	40%	60%	80%
$S_f[\ddot{r}, \ddot{y}_0]$ (%)	99.45	98.64	98.48	98.97	99.17
$S_t[\ddot{r}, \ddot{y}_0]$ (%)	94.14	91.96	92.98	94.25	95.22

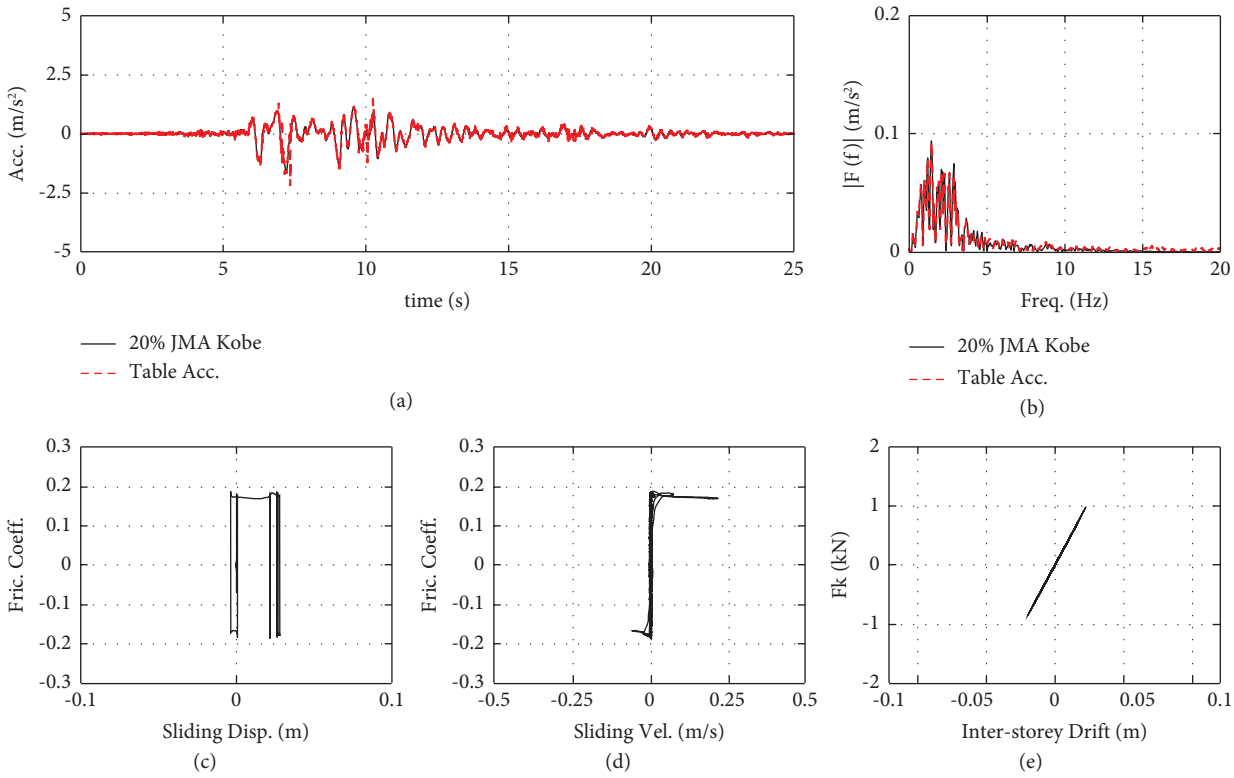

Figure 16: Experimental results of NSBC based on Linear Model 1.5 for 20% JMA Kobe motion: (a) time history of the table acceleration, (b) Fourier amplitude spectra of the table acceleration, (c) friction coefficient vs. sliding displacement, (d) friction coefficient vs. sliding velocity, and (e) shear force vs. inter-storey drift in the superstructure.

Figure 4(a). The steel plates demonstrated the flexibility of a building structure and functioned as an element that displayed nonlinear characteristics, similar to those shown in Figure 4(b). The set of blocks shown in Figure 12(d) had an iron at its centre, which was placed on each corner of the sliding mass. The flat area (20×20 mm) on the iron block, as shown in Figure 12(d), was attached to the bases, forming the sliding interface of the sliding structure. This interface was lubricated with graphite to achieve a friction coefficient of approximately 0.2. With this lubrication, 0.06 kg of graphite was scattered on the mortar base for each iron block, as shown in Figure 12(e). During the preparation of this experiment, the first and second masses were measured as $m_1 = 225$ kg and $m_2 = 200$ kg, respectively, and the experimental rigs directly placed on the table were $m_{0\alpha} = 115$ kg, resulting in $m_0 = m_{0b} + m_{0\alpha} = 315$ kg. Based on the total weight of the sliding structure, $m_1 + m_2 = 425$ kg, and the contact pressure at the interface became 2.6 N/mm^2.

The shake table had a magnetostrictive displacement transducer and two servo accelerometers for control. The sliding mass was equipped with four wire displacement transducers placed at its corners to measure its sliding displacement and two strain gauge accelerometers attached to the mass for its acceleration. The superstructure was equipped with two wire displacement transducers placed on protection stands to measure its interstorey drift and two strain gauge accelerometers on the second mass.

System identification tests were performed with a band-limited random excitation containing frequency components of 0.1–50 Hz, with two different amplitudes of 10.0 and 2.0 mm. The dynamics of the table displacement and control input signal obtained for the two amplitude cases are illustrated in Figure 13.

The dynamics in Figure 13(a), which were obtained with an amplitude of 10.0 mm, was modelled by the following expression:

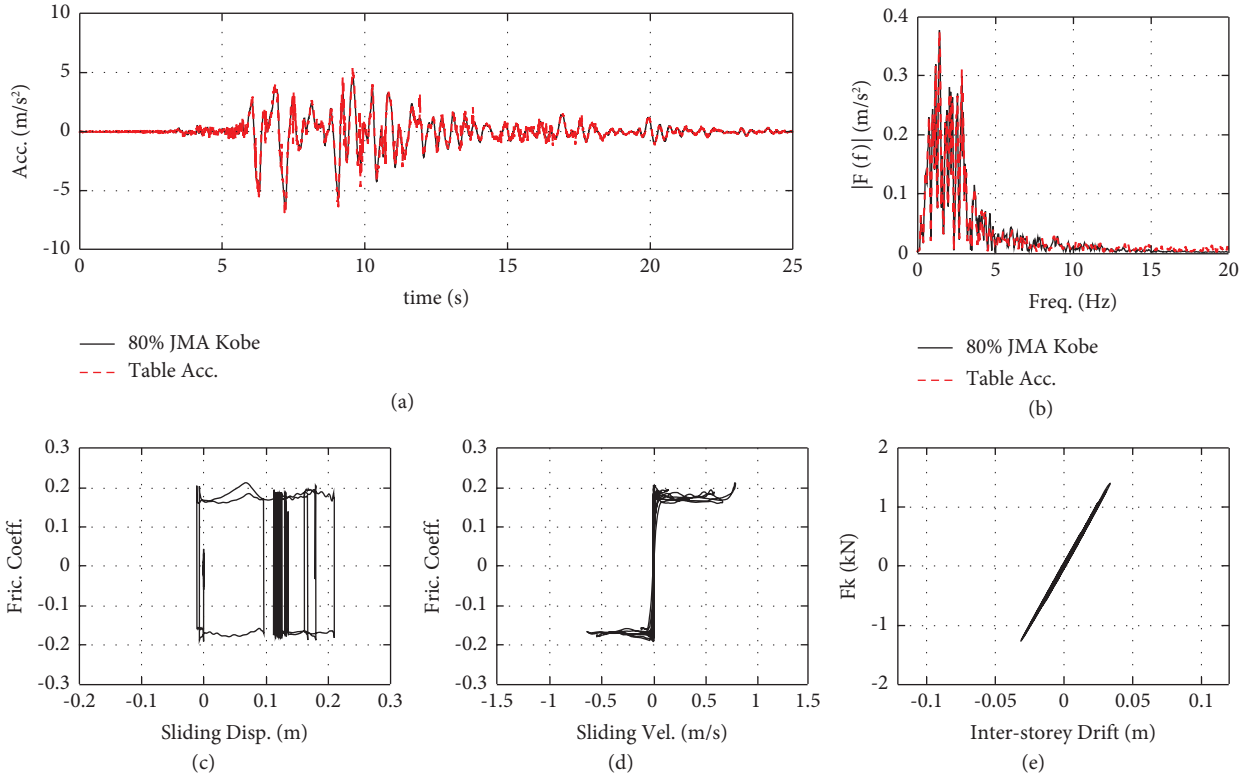

FIGURE 17: Experimental results of NSBC based on Linear Model 1.5 for 80% JMA Kobe motion: (a) time history of the table acceleration, (b) Fourier amplitude spectra of the table acceleration, (c) friction coefficient vs. sliding displacement, (d) friction coefficient vs. sliding velocity, and (e) shear force vs. inter-storey drift in the superstructure.

$$\begin{cases} G_{0d}(s)\left(=G_{0/u}(s)\right)=\dfrac{131.6s^2+78.96s+2.829e04}{s^4+9.665s^3+431.5s^2+1980s+2.829e04}, \\ G_{0a}(s)=s^2G_{0d}(s). \end{cases} \tag{28}$$

Based on $\{m_0, m_1, m_2\} = \{315,225,200\}$ kg and equation (26), the equivalent table parameters were found to be $c_0 = 4.78$ kNs/m and $k_0 = 71.06$ kN/m, and the superstructure was found to have the following parameters: $c_2 = 120$ Ns/m and $k_2 = 43.00$ kN/m.

In the system identification test with an amplitude of 2.0 mm, as shown in Figure 13(b), the obtained dynamics slightly differed from those obtained with an amplitude of 10.0 mm, indicating that the shake table had some nonlinear characteristics depending on its amplitude.

Based on the identified parameters, Linear Model 1 was built using equation (26) with the following parameters: $\{\overline{m}_0, \overline{c}_0, \overline{k}_0, \overline{m}_1, \overline{m}_2, \overline{c}_2, \overline{k}_2\} = \{m_0, c_0, k_0, m_1, m_2, c_2, k_2\}$. This resulted in a transfer function identical to that expressed by equation (28). To improve the stability margin of Linear Model 1, Linear Model 1.5 was alternatively built using $\{\overline{m}_0, \overline{c}_0, \overline{k}_0, \overline{m}_1, \overline{m}_2, \overline{c}_2, \overline{k}_2\} = \{m_0, 1.5c_0, 1.5k_0, m_1, m_2, c_2, k_2\}$.

4.2. Shake Table Experiments with Linear Model 1. Shake table experiments based on NSBC and IBC were conducted using Linear Model 1. Based on this model, the NSBC controllers were designed using equation (15) with $\overline{G}(s) = G_{0a}(s)$ for the control input signal in equation (14). The bandpass filter $F_\sigma(s)$ in equation (15) was identical to that used in the numerical simulations. IBC was executed by NSBC with $K_\sigma(s) = K_e(s) = 0$.

4.2.1. Experimental Results of IBC with Linear Model 1. Shake table experiments with IBC were performed for two amplitudes of 10% and 20%. The results are summarised in Table 4. The results for the 20% excitation are illustrated in Figure 14. The sliding interface had a friction coefficient of approximately 0.2, as observed in Figure 14(c).

At 10% excitation, the structure did not slide, and nonlinear characteristics that occurred in this experiment were limited. The control accuracies in Table 4 are $S_f = 94.10\%$ and $S_t = 81.82\%$, which were much lower than those of the numerical simulation in Section 3.2.1. This is attributed to the nonlinear characteristics of the shake table.

At 20% excitation, the structure clearly slid, as shown in Figure 14, and caused control degradation, resulting in $S_f = 79.43\%$ and $S_t = 61.65\%$, which are again worse than those of the numerical simulations.

It should be noted that experiments with larger excitations were not performed because their poor results were deduced from the numerical simulation and the experimental results of 10% and 20% excitations.

4.2.2. Experimental Results of NSBC with the Linear Model 1. Shake table experiments with NSBC were scheduled to be performed using JMA Kobe motion with the two amplitudes of 10% and 20%. However, NSBC with Linear Model 1 became unstable in the experiment with 10% excitation, as shown in Figure 15. This can be attributed to the nonlinear characteristics of the table. This result confirms the unsuitability of Linear Model 1 for the shake table experiments in this study.

4.3. Shake Table Experiments with Linear Model 1.5. Shake table experiments based on NSBC were conducted using Linear Model 1.5. Based on this linear model, NSBC controllers were designed using equation (15) with $\overline{G}(s) = G_{0a}(s)$ for the control input signal in equation (14). The bandpass filter $F_\sigma(s)$ was the same as the one one used in Linear Model 1.

Shake table experiments based on NSBC using Linear Model 1.5 were conducted with JMA Kobe motion with the amplitudes: {10%, 20%, 40%, 60%, and 80%}. The experimental results are summarised in Table 5, and the detailed results of the 20% and 80% excitations are illustrated in Figures 16 and 17, respectively. Note that the experiment with 100% excitation was not executed because the 80% excitation resulted in a large sliding displacement, which was near the limit of the allowable range of sliding.

NSBC based on Linear Model 1.5 maintained stability in all experiments with different amplitudes, unlike NSBC based on Linear Model 1, which became unstable at 10% excitation. This simply demonstrates the superiority of Linear Model 1.5 over Linear Model 1.

At 10% excitation, NSBC based on Linear Model 1.5 achieved the expected control with sufficient accuracies of $S_f = 99.45\%$ and $S_t = 94.14\%$. During this experiment, the structure did not slide on the table owing to the small excitation. Although the 20% excitation clearly caused the structure to slide on the table, as shown in Figure 16, its table acceleration was sufficiently close to the reference signal in both time and frequency domains. The control accuracies were $S_f = 98.64\%$ and $S_t = 91.96$, which were remarkably better than IBC results for 20% excitation as shown in Table 4.

In the experiments with larger excitations, the control accuracies were similar to or better than those with smaller excitations, as shown in Table 5. At 80% excitation, the table acceleration was accurately controlled, as shown in Figures 17(a) and 17(b), with high accuracies of $S_f = 99.17\%$ and $S_t = 95.22\%$, which are the best results among all the experiments conducted in this study. S_t at this excitation was the highest in Table 5, because the influence of the noise contaminating the table acceleration decreased as the excitation amplitude increased.

In addition to the accurate control of the shake table shown in Figures 17(a) and 17(b), the responses of the sliding structure in Figure 17(c)–17(e) reasonably match the numerical results of the sliding structure in Figure 6. This result also supports the reliability of the experiments conducted with NSBC based on Linear Model 1.5.

5. Conclusions

This study examined the performance of NSBC in shake table experiments with a sliding structure based on a graphite-lubricated interface. Its high performance was verified through numerical simulations and actual experiments. The results obtained in this study are summarised as follows:

(i) As building a linear model of a controlled system is essential for NSBC, this study introduced its design for a shake table with a sliding structure. The linear model is built based on the controlled system during the stick state of a sliding structure rather than the slip state. The designs of the linear model and NSBC controllers were exemplified by a shake table and a sliding structure, which consists of sliding mass and an N-DOF superstructure. In addition, this study introduced an approximate stability analysis of NSBC for such shake table experiments, in which the controlled system is represented by table dynamics during the slip state of the sliding structure.

(ii) To enhance the robustness of NSBC against uncertainty within a shake table, this study additionally introduced a linear model design in which the model parameters corresponding to damping and stiffness of the shake table are intentionally assumed to be larger than the identified values. Its effectiveness was demonstrated by the stability analysis for two different models: Linear Model 1, built using the exact initial parameters of the controlled system, and Linear Model 1.5, built using 1.5 times the damping and stiffness values corresponding to its shake table part.

(iii) Numerical simulations were performed for shake table experiments with a sliding structure consisting of an SDOF superstructure and a sliding mass, and a sliding interface with a friction coefficient of 0.22. In the simulations, IBC, which is a basic compensation method for shake table control, produced satisfactory results only when the sliding structure remained in the stick state, and its control accuracy significantly deteriorated as the sliding amplitude increased. Contrarily, NSBC accurately realised an expected earthquake excitation with high accuracy: almost 100%, even when the structure on the table slid substantially. Linear Models 1 and 1.5 did not exhibit significant differences in terms of control accuracies.

(iv) In the experiments, a sliding structure consisting of a one-storey steel structure and a sliding mass was placed on a sliding interface lubricated with

graphite, realising a friction coefficient of approximately 0.2. First, NSBC controllers were built using Linear Model 1 with the exact parameters of the controlled system obtained from a system identification test. However, a shake table experiment using NSBC with this model became unstable, mainly because of the nonlinear characteristics within the table. Contrarily, NSBC based on Linear Model 1.5 maintained stability and achieved an expected earthquake excitation with high accuracy, i.e., over 99.6% and 95.2% in the frequency and time domains, respectively.

(v) In this study, NSBC with a reasonable linear model achieved accurate control of the shake table even when the table sustained a sliding structure whose weight (425 kg) was 2.1 times greater than the bare table weight (200 kg). This study clarified that NSBC can solve the problem of control degradation of shake tables with heavy sliding structures.

The stability analysis of NSBC for shake table experiments involving the sliding phenomenon must be further elaborated for more accurate assessments. Furthermore, systematic designs of the linear model and NSBC controllers should be constructed. This study focused on examining the control performance of NSBC for shake table experiments with a single-storey sliding structure, based on the sliding interface having a friction coefficient of approximately 0.2. Its performance for different friction coefficients can be found in the study with a rigid sliding mass [65]. We will further investigate the control performance of NSBC in shake table experiments with sliding structures with multistorey superstructures. As applications of NSBC are currently limited to single-axis shake tables, we will investigate the applicability of NSBC to multi-axial shake tables.

Data Availability

The data used to support the findsing of this study are available from the corresponding author on reasonable request.

Conflicts of Interest

The authors declare that there are no conflicts of interest regarding the publication of this paper.

Acknowledgments

This study was supported by the research grants (Nos. 20H02228 and 22K18838) from the Japan Society for the Promotion of Science.

References

[1] R. T. Severn, "The development of shaking tables-A historical note," *Earthquake Engineering & Structural Dynamics*, vol. 40, no. 2, pp. 195–213, 2011.

[2] M. Nakashima, T. Nagae, R. Enokida, and K. Kajiwara, "Experiences, accomplishments, lessons, and challenges of E-defense—tests using world's largest shaking table," *Japan Archit Rev*, vol. 1, no. 1, pp. 4–17, 2018.

[3] J. Yao, M. Dietz, R. Xiao, H. Yu, T. Wang, and D. Yue, "An overview of control schemes for hydraulic shaking tables," *Journal of Vibration and Control*, vol. 22, no. 12, pp. 2807–2823, 2016.

[4] Y. Tagawa and K. Kajiwara, "Controller development for the E-Defense shaking table," *Journal of Systems and Control Engineering*, vol. 221, no. 2, pp. 171–181, 2007.

[5] M. Blondet and C. Esparza, "Analysis of shaking table-structure interaction effects during seismic simulation tests," *Earthquake Engineering & Structural Dynamics*, vol. 16, no. 4, pp. 473–490, 1988.

[6] J. P. Conte and T. L. Trombetti, "Linear dynamic modeling of a uni-axial servo-hydraulic shaking table system," *Earthquake Engineering & Structural Dynamics*, vol. 29, no. 9, pp. 1375–1404, 2000.

[7] P. C. Chen, C. T. Lai, and K. C. Tsai, "A control framework for uniaxial shaking tables considering tracking performance and system robustness," *Structural Control and Health Monitoring*, vol. 24, no. 11, Article ID e2015, 2017.

[8] A. R. Plummer, "A detailed dynamic model of a six-Axis shaking table," *Journal of Earthquake Engineering*, vol. 12, no. 4, pp. 631–662, 2008.

[9] X. Gao and S. J. Dyke, "Modeling and control of actuators for high performance structural dynamic testing," *Smart Materials and Structures*, vol. 23, no. 5, Article ID 055008, 2014.

[10] Y. Qian, G. Ou, A. Maghareh, and S. J. Dyke, "Parametric identification of a servo-hydraulic actuator for real-time hybrid simulation," *Mechanical Systems and Signal Processing*, vol. 48, no. 1-2, pp. 260–273, 2014.

[11] N. Nakata and E. Krug, "Computational framework for effective force testing and a compensation technique for nonlinear actuator dynamics," *Structural Control and Health Monitoring*, vol. 21, no. 5, pp. 756–773, 2013.

[12] P. Righettini, R. Strada, S. Valilou, and E. KhademOlama, "Nonlinear model of a servo-hydraulic shaking table with dynamic model of effective bulk modulus," *Mechanical Systems and Signal Processing*, vol. 110, pp. 248–259, 2018.

[13] J. Ramírez-Senent, J. H. García-Palacios, and I. M. Díaz, "Shaking table control via real-time inversion of hydraulic servoactuator linear state-space model," *Journal of Systems and Control Engineering*, vol. 235, no. 9, pp. 1650–1666, 2021.

[14] A. R. Plummer, "Control techniques for structural testing: a review," *Journal of Systems and Control Engineering*, vol. 221, no. 2, pp. 139–169, 2007.

[15] T. Horiuchi, M. Inoue, T. Konno, and W. Yamagishi, "Development of a real-time hybrid experimental system using a shaking table. (Proposal of experiment concept and feasibility study with rigid secondary system)," *JSME Int J Ser C*, vol. 42, no. 2, pp. 255–264, 1999.

[16] S. K. Lee, E. C. Park, K. W. Min, and J. H. Park, "Real-time substructuring technique for the shaking table test of upper substructures," *Engineering Structures*, vol. 29, no. 9, pp. 2219–2232, 2007.

[17] R. Zhang, B. M. Phillips, S. Taniguchi, M. Ikenaga, and K. Ikago, "Shake table real-time hybrid simulation techniques for the performance evaluation of buildings with inter-story isolation," *Structural Control and Health Monitoring*, vol. 24, no. 10, Article ID e1971, 2017.

[18] Z. Tang, M. Dietz, Y. Hong, and Z. Li, "Performance extension of shaking table-based real-time dynamic hybrid testing through full state control via simulation," *Structural Control and Health Monitoring*, vol. 27, no. 10, Article ID e2611, 2020.

[19] R. Enokida, "Basic examination of two substructuring schemes for shake table tests," *Structural Control and Health Monitoring*, vol. 27, no. 4, Article ID e2497, 2020.

[20] Y. Mukai, A. Yokoyama, K. Fushihara, T. Fujinaga, and H. Fujitani, "Real-time hybrid test using two-individual actuators to evaluate seismic performance of RC frame model controlled by AMD," *Front Built Environ*, vol. 6, p. 145, 2020.

[21] Y. Tian, X. Shao, H. Zhou, and T. Wang, "Advances in real-time hybrid testing technology for shaking table substructure testing," *Front Built Environ*, vol. 6, p. 123, 2020.

[22] D. P. Stoten and H. Benchoubane, "Empirical studies of an MRAC algorithm with minimal controller synthesis," *International Journal of Control*, vol. 51, no. 4, pp. 823–849, 1990.

[23] D. P. Stoten and H. Benchoubane, "Robustness of a minimal controller synthesis algorithm," *International Journal of Control*, vol. 51, no. 4, pp. 851–861, 1990.

[24] Y. D. Landau, *Adaptive Control: The Model Reference Approach*, Marcel Dekker, Inc, New York, NY, USA, 1979.

[25] D. P. Stoten and E. G. Gómez, "Adaptive control of shaking tables using the minimal control synthesis algorithm," *Philosophical Transactions of the Royal Society of London,Series A: Mathematical, Physical and Engineering Sciences*, vol. 359, no. 1786, pp. 1697–1723, 2001.

[26] D. P. Stoten and N. Shimizu, "The feedforward minimal control synthesis algorithm and its application to the control of shaking-tables," *Journal of Systems and Control Engineering*, vol. 221, no. 3, pp. 423–444, 2007.

[27] A. O. Gizatullin and K. A. Edge, "Adaptive control for a multi-axis hydraulic test rig," *Journal of Systems and Control Engineering*, vol. 221, no. 2, pp. 183–198, 2007.

[28] S. Gang, Z. Zhen-Cai, Z. Lei et al., "Adaptive feed-forward compensation for hybrid control with acceleration time waveform replication on electro-hydraulic shaking table," *Control Engineering Practice*, vol. 21, no. 8, pp. 1128–1142, 2013.

[29] T. Yachun, P. Peng, Z. Dongbin, and Z. Yi, "A two-loop control method for shaking table tests combining model reference adaptive control and three-variable control," *Front Built Environ*, vol. 4, p. 54, 2018.

[30] G. Shen, X. Li, Z. Zhu, Y. Tang, W. Zhu, and S. Liu, "Acceleration tracking control combining adaptive control and off-line compensators for six-degree-of-freedom electro-hydraulic shaking tables," *ISA Transactions*, vol. 70, pp. 322–337, 2017.

[31] K. P. Ryu and A. M. Reinhorn, "Real-time control of shake tables for nonlinear hysteretic systems," *Structural Control and Health Monitoring*, vol. 24, no. 2, Article ID e1871, 2017.

[32] J. Liu, B. Qiao, X. Zhang, R. Yan, and X. Chen, "Adaptive vibration control on electrohydraulic shaking table system with an expanded frequency range: theory analysis and experimental study," *Mechanical Systems and Signal Processing*, vol. 132, pp. 122–137, 2019.

[33] S. Y. Chu, S. C. Lo, and M. C. Chang, "Real-time control performance of a model-reference adaptive structural control system under earthquake excitation," *Structural Control and Health Monitoring*, vol. 17, no. 2, pp. 198–217, 2010.

[34] V. Mañosa, F. Ikhouane, and J. Rodellar, "Control of uncertain non-linear systems via adaptive backstepping," *Journal of Sound and Vibration*, vol. 280, no. 3-5, pp. 657–680, 2005.

[35] Y. Hacioglu and N. Yagiz, "Adaptive backstepping control with estimation for the vibration isolation of buildings," *Journal of Vibration and Control*, vol. 18, no. 13, pp. 1996–2005, 2012.

[36] J. Yao and W. Deng, "Active disturbance rejection adaptive control of uncertain nonlinear systems: theory and application," *Nonlinear Dynamics*, vol. 89, no. 3, pp. 1611–1624, 2017.

[37] J. Shan, Y. Ouyang, and W. Shi, "Adaptive control of earthquake-excited nonlinear structures with real-time tracking on prescribed performance criteria," *Structural Control and Health Monitoring*, vol. 25, no. 10, p. e2247, 2018.

[38] N. Nakata, "Acceleration trajectory tracking control for earthquake simulators," *Engineering Structures*, vol. 32, no. 8, pp. 2229–2236, 2010.

[39] B. M. Phillips, N. E. Wierschem, and B. F. Spencer, "Model-based multi-metric control of uniaxial shake tables," *Earthquake Engineering & Structural Dynamics*, vol. 43, no. 5, pp. 681–699, 2014.

[40] A. R. Plummer, "Model-based motion control for multi-axis servohydraulic shaking tables," *Control Engineering Practice*, vol. 53, pp. 109–122, 2016.

[41] A. Najafi and B. F. Spencer, "Modified model-based control of shake tables for online acceleration tracking," *Earthquake Engineering & Structural Dynamics*, vol. 49, no. 15, pp. 1721–1737, 2020.

[42] R. Enokida, I. Takewaki, and D. Stoten, "A nonlinear signal-based control method and its applications to input identification for nonlinear SIMO problems," *Journal of Sound and Vibration*, vol. 333, no. 24, pp. 6607–6622, 2014.

[43] R. Enokida, "Stability of nonlinear signal-based control for nonlinear structural systems with a pure time delay," *Structural Control and Health Monitoring*, vol. 26, no. 8, Article ID e2365, 2019.

[44] R. Enokida and K. Kajiwara, "Nonlinear signal-based control for single-axis shake tables supporting nonlinear structural systems," *Structural Control and Health Monitoring*, vol. 26, no. 9, Article ID e2376, 2019.

[45] R. Enokida, "Enhancement of nonlinear signal-based control to estimate earthquake excitations from absolute acceleration responses of nonlinear structures," *Mechanical Systems and Signal Processing*, vol. 181, no. 1, Article ID 109486, 2022.

[46] R. Enokida and K. Kajiwara, "Nonlinear signal-based control with an error feedback action for nonlinear substructuring control," *Journal of Sound and Vibration*, vol. 386, pp. 21–37, 2017.

[47] R. Enokida and K. Kajiwara, "Nonlinear substructuring control for parameter changes in multi-degree-of-freedom systems," *Journal of Sound and Vibration*, vol. 407, pp. 63–81, 2017.

[48] R. Enokida, "Nonlinear substructuring control for simultaneous control of acceleration and displacement in shake table substructuring experiments," *Structural Control and Health Monitoring*, vol. 29, no. 2, Article ID e2882, 2022.

[49] R. Enokida and K. Kajiwara, "Simple piecewise linearisation in time series for time-domain inversion to estimate physical parameters of nonlinear structures," *Structural Control and Health Monitoring*, vol. 27, no. 10, Article ID e2606, 2020.

[50] N. Mostaghel, M. Hejazi, and J. Tanbakuchi, "Response of sliding structures to harmonic support motion," *Earthquake Engineering & Structural Dynamics*, vol. 11, no. 3, pp. 355–366, 1983.

[51] N. Mostaghel and J. Tanbakuchi, "Response of sliding structures to earthquake support motion," *Earthquake Engineering & Structural Dynamics*, vol. 11, no. 6, pp. 729–748, 1983.

[52] J. M. Kelly, "Aseismic base isolation: review and bibliography," *Soil Dynamics and Earthquake Engineering*, vol. 5, no. 4, pp. 202–216, 1986.

[53] A. Mokha, M. C. Constantinou, A. M. Reinhorn, and V. A. Zayas, "Experimental study of friction-pendulum isolation system," *Journal of Structural Engineering*, vol. 117, no. 4, pp. 1201–1217, 1991.

[54] D. M. Fenz and M. C. Constantinou, "Behaviour of the double concave friction pendulum bearing," *Earthquake Engineering & Structural Dynamics*, vol. 35, no. 11, pp. 1403–1424, 2006.

[55] T. C. Becker and S. A. Mahin, "Experimental and analytical study of the bi-directional behavior of the triple friction pendulum isolator," *Earthquake Engineering & Structural Dynamics*, vol. 41, no. 3, pp. 355–373, 2012.

[56] P. M. Calvi and G. M. Calvi, "Historical development of friction-based seismic isolation systems," *Soil Dynamics and Earthquake Engineering*, vol. 106, pp. 14–30, 2018.

[57] A. Turer and B. Özden, "Seismic base isolation using low-cost scrap tire pads (STP)," *Materials and Structures*, vol. 41, no. 5, pp. 891–908, 2008.

[58] M. Spizzuoco, A. Calabrese, and G. Serino, "Innovative low-cost recycled rubber–fiber reinforced isolator: experimental tests and finite element analyses," *Engineering Structures*, vol. 76, pp. 99–111, 2014.

[59] A. Calabrese, M. Spizzuoco, G. Serino, G. Della Corte, and G. Maddaloni, "Shaking table investigation of a novel, low-cost, base isolation technology using recycled rubber," *Structural Control and Health Monitoring*, vol. 22, no. 1, pp. 107–122, 2015.

[60] A. Tsiavos, N. A. Alexander, A. Diambra et al., "A sand-rubber deformable granular layer as a low-cost seismic isolation strategy in developing countries: experimental investigation," *Soil Dynamics and Earthquake Engineering*, vol. 125, Article ID 105731, 2019.

[61] R. Enokida, T. Nagae, M. Ikenaga, M. Inami, and M. Nakashima, "Application of graphite lubrication for column base in free standing steel structure," *Journal of Structural and Construction Engineering (Transactions of AIJ)*, vol. 78, no. 685, pp. 435–444, 2013.

[62] R. P. Nanda, M. Shrikhande, and P. Agarwal, "Low-cost base-isolation system for seismic protection of rural buildings," *Practice Periodical on Structural Design and Construction*, vol. 21, no. 1, Article ID 04015001, 2016.

[63] F. Barbagallo, I. Hamashima, H. Hu, M. Kurata, and M. Nakashima, "Base shear capping buildings with graphite-lubricated bases for collapse prevention in extreme earthquakes," *Earthquake Engineering & Structural Dynamics*, vol. 46, no. 6, pp. 1003–1021, 2017.

[64] R. Enokida and T. Nagae, "Seismic damage reduction of a structural system based on nontraditional sliding interfaces with graphite lubrication," *Journal of Earthquake Engineering*, vol. 22, no. 4, pp. 666–686, 2018.

[65] R. Enokida, K. Ikago, J. Guo, and K. Kajiwara, "Nonlinear signal–based control for shake table experiments with sliding masses," *Earthquake Engineering & Structural Dynamics*, vol. 52, no. 6, pp. 1908–1931, 2023.

[66] D. Karnopp, "Computer simulation of stick-slip friction in mechanical dynamic systems," *Journal of Dynamic Systems, Measurement, and Control*, vol. 107, no. 1, pp. 100–103, 1985.

[67] B. Armstrong-Hélouvry, P. Dupont, and C. C. De Wit, "A survey of models, analysis tools and compensation methods for the control of machines with friction," *Automatica*, vol. 30, no. 7, pp. 1083–1138, 1994.

[68] P. Olejnik, J. Awrejcewicz, and M. Fečkan, *Modeling, analysis and control of dynamical systems*, World Scientific Series on Nonlinear Science Series A, World Scientific Publishing Co. Pte. Lt, vol. 92, Singapore, 2017.

[69] S. Kato, K. Yamaguchi, and T. Matsubayashi, "Stick-slip motion of machine tool slideway," *Journal of Engineering for Industry*, vol. 96, no. 2, pp. 557–566, 1974.